THE ASTROPHYSICAL JOURNAL, 487:867–884, 1997 October 1

ROSAT PSPC OBSERVATIONS OF 27 NEAR–MAIN-SEQUENCE B STARS

D. H. COHEN,[1,2] J. P. CASSINELLI,[1] AND J. J. MACFARLANE[1,2]

Received 1996 December 10; accepted 1997 May 9

ABSTRACT

In this paper, we report on *ROSAT* Position Sensitive Proportional Counter (PSPC) observations of 27 near–main-sequence B stars made with unprecedented sensitivity. Contrary to the results of previous surveys, it is found that 75% of the sample stars are X-ray sources, albeit most at modest levels. The X-ray luminosities of the program stars range from 5.6×10^{27} up to 2.2×10^{32} ergs s^{-1}. We find that L_X/L_{Bol} decreases abruptly beyond about B0 and stabilizes at $L_X/L_{Bol} \approx 10^{-8.5}$ by about B2, with seven nondetections at B2 and later. For the B0 and B1 stars, our modeling suggests that wind attenuation of the X-ray photons is significant, so that the emitted X-ray luminosity, corrected for this attenuation, actually exceeds $10^{-7}L_{Bol}$ in some cases. Presumably, this situation is even more severe for O stars; thus, the well-known $L_X/L_{Bol} \approx 10^{-7}$ law simply may be an artifact of the neglect of wind attenuation. The *ROSAT* PSPC observations of most of the B stars are very soft, with the notable exception of τ Sco (B0 V). The wind emission measure filling factors that we find for the very early B stars are rather large (roughly 0.1–1). This could be brought into line with theoretical calculations of the line-force instability, wind-shock mechanism if the mass-loss rates of these stars are a few times higher than theory currently predicts. However, the X-rays from stars later than B2 require filling factors greater than unity and thus cannot be produced by any radiation-driven wind-shock mechanism because there is simply not enough wind material to produce the observed X-rays. It is possible that mid- to late-B stars represent some kind of transition to, or hybrid of, wind and coronal X-ray mechanisms.

Subject headings: radiation mechanisms: thermal — shock waves — stars: atmospheres — stars: early-type — X-rays: stars

1. INTRODUCTION

Most stars are X-ray sources, with one of two X-ray production mechanisms operating: wind shocks in O and very early B stars (B0 and B1), and coronal emission in late-type stars. The level of X-ray emission is expected to decrease sharply in intermediate spectral types (mid-B to mid-F), where neither strong stellar winds nor convection-driven coronae are thought to exist. However, several recent observations have shown low to moderate levels of X-ray emission and UV chromospheric activity in a few stars in this intermediate spectral range (Schmitt et al. 1993; Berghöfer & Schmitt 1994a; Walter, Matthews, & Linsky 1995; Freire Ferrero et al. 1995). The transition from the shock-generated X-rays of O and very early B stars to the widely varied X-ray properties of mid-B stars (considered in this paper to be roughly B3 and later) is poorly understood, and its definition is the purpose of this paper. To accomplish this, we obtained pointed *ROSAT* Position Sensitive Proportional Counter (PSPC) observations of 27 near–main-sequence B stars (luminosity classes III, IV, and V, referred to as "B V stars") ranging in spectral type from B0, which have strong stellar winds, to B7, which are predicted to have very weak winds. We modeled these data to see if the wind-shock paradigm can explain the observed X-ray properties of B V stars and to what extent other mechanisms must be invoked to explain the observational data.

1.1. *General Properties and Stellar Winds of B V Stars*

Several interesting classes of stars exist among B V stars, and the processes that occur in these objects may be relevant to the generation of X-ray emission both in these subclasses and in B V stars in general. Photospheric pulsations are known to occur in many B stars, including, but not limited to, β Cephei variables (Smith 1980; Waelkens & Rufener 1985; Sterken & Jerzykiewicz 1993). Emission-line (Be) stars have disks and active photospheric and mass ejection episodes, and rapid rotation appears to play a crucial role in the Be phenomenon. Among the mid- and late-type B stars, several categories of chemically peculiar stars exist, and some of these have very strong ($B \sim 1$ kG) magnetic fields (Bohlender 1994). The relevant properties—pulsation, rapid rotation, and possibly magnetic fields—also exist to one extent or another in normal B V stars. All of these properties have implications for X-ray emission processes in B V stars, both those involving wind shocks and those that do not. Pulsation, rotation, and episodes of strong and variable mass ejections could all affect wind-shock mechanisms, while rotation and magnetic fields are prerequisites for coronal activity.

Winds in early-type stars are driven by radiation pressure acting on many spectral lines. This theory has been very successful in describing the time-average properties of O and very early B stars (Abbott 1982; Kudritzki et al. 1992), but the application of radiation-driven wind theory to B V stars is problematic. Making accurate calculations of radiation pressure in these lower density winds is difficult because the ionization balance is relatively unconstrained by observations, and the calculations give widely divergent results. If X-ray photoionization is as important as the calculations indicate (MacFarlane, Cohen, & Wang 1994), then the high-ion lines that have been commonly observed in the UV in B V stars (C IV, N V, and Si IV) may be present only in trace amounts. If this is so, then UV absorption-line data for B V stars would not yield any useful constraints on the wind properties.

[1] University of Wisconsin at Madison, Department of Astronomy, 475 North Charter Street, Madison, WI 53706; cohen@duff.astro.wisc.edu.
[2] University of Wisconsin at Madison, Fusion Technology Institute, 1500 Johnson Drive, Madison, WI 53706.

Although spherically symmetric, time-independent models are often computed, and generally provide good agreement with the observed time-average properties of the strong winds of O stars, variability is seen in the optical and UV wind spectral lines of many of these objects. This variability includes large-scale activity evidenced as discrete absorption components (DACs) that remain coherent for many hours as well as smaller scale, faster variability (e.g., Massa et al. 1995; Kaper et al. 1996). The line shapes of saturated P Cygni profiles imply that the stellar winds have nonmonotonic velocity fields (Lucy 1983), and comparisons of the IR and radio excesses show that some O stars have clumpy winds (Runacres & Blomme 1996). Taken together, these observations indicate that radiation-driven winds are time dependent with variability, on both long and short timescales, and structure, on both large and small spatial scales, in which significant amounts of energy may be dissipated. Such observations in B V stars are much rarer because of the low densities of their winds, but presumably similar types of variability exist in the winds of these objects too.

1.2. *Wind Shocks and X-Rays*

The line-driving mechanism in winds is inherently unstable (Lucy & Solomon 1970), and this radiation-force instability has been explored numerically in recent years (Owocki, Castor, & Rybicki 1988; Cooper 1994; Feldmeier 1995). Numerical simulations that allow instabilities to grow from very small seed perturbations produce short-timescale stochastic variability and indicate that many shocks form throughout the wind (Cooper 1994). Some of these shocks have jump velocities of several hundred km s^{-1}, heating plasma to temperatures up to $\sim 10 \times 10^6$ K (~ 10 MK), although most shocks in the simulations are weaker. Shocks may be even stronger, and periodic, if large-amplitude photospheric sound waves are assumed as an ad hoc perturbing agent (Feldmeier, Puls, & Pauldrach 1997b). And, in general, as MacFarlane & Cassinelli (1989) have demonstrated, given arbitrary freedom to assign boundary conditions, wind shocks of very high temperatures and emission measures can be produced. Although the radiation-force instability is the most commonly investigated mechanism for generating wind shocks, it is by no means the only one. For example, the large-scale variability represented by DACs cannot be explained by the radiation-force instability, but modeling suggests that they may be explained by corotating interaction regions (CIRs) that can lead to wind shocks and X-ray emission also (Mullan 1984; Cranmer & Owocki 1996).

The numerical calculations of the radiation-force instability have been performed primarily for O supergiants. These show that shocks formed directly by the line-force instability mechanism produce 1–2 orders of magnitude too little hot gas (Cooper 1994; Feldmeier 1995; Feldmeier et al. 1997b). However, collisions between dense shells farther out in the wind flow can produce roughly the correct amount of X-ray emission in the very dense winds of O supergiants if large photospheric perturbations are included as a lower boundary condition (Feldmeier et al. 1997b). The application of the instability mechanism itself and the secondary shell collisions to B V stars is uncertain, however, because of their very low wind densities. For very late main-sequence O stars (Cooper 1994) and early-B bright giants (Cohen et al. 1996), which have wind densities about 100 times less than O supergiants but significantly greater than B V stars, the shocks generated within a few stellar radii of the photosphere by the line-force instability mechanism can account for the observed X-ray fluxes. The numerical simulations tend to produce temperature distributions in the postshock gas that are weighted toward lower temperatures, which is generally in accord with observations (Cohen et al. 1996).

Besides the overall X-ray flux levels and derived temperature distributions, the degree of wind attenuation of X-rays is another observational test of the applicability of wind-shock models to early-type stars. Recent moderate-resolution observations show evidence for wind attenuation of the X-rays consistent with the predictions of the wind-shock model (Corcoran et al. 1993; Hillier et al. 1993; Cohen et al. 1996). Indeed, for ζ Pup (O4 If), much of the observed soft X-ray emission arises near or above $100R_*$ (Hillier et al. 1993). However, analysis of the O VI profile of ζ Pup shows that a significant amount of the X-ray emission is generated within a few stellar radii of the photosphere (MacFarlane et al. 1993). These two pictures are generally consistent because Hillier et al. (1993) claim that only about 5% of the emitted X-rays escape the stellar wind. Observations of B supergiants indicate that only about half of the generated X-rays emerge unattenuated from the stellar wind (Cassinelli et al. 1981). Recently, the *Extreme-Ultraviolet Explorer* (*EUVE*) and *ROSAT* data from ϵ CMa (B2 II) show that only about 20% of the EUV emission and 80% of the X-ray emission emerge from the stellar wind without being absorbed (Cohen et al. 1996). Because of the precipitous decline of the mass-loss rate with decreasing effective temperature, very early B V stars should have winds that are only marginally optically thick to X-rays. And stars later than about B1.5 should have winds that are optically thin down nearly to the photosphere. This means that the observed X-rays from B V stars sample almost all of the wind, not just the extreme outer layers as is the case for X-ray observations of O stars.

1.3. *X-Ray Properties of Early-Type Stars*

Both the *Einstein* and *ROSAT* all-sky surveys have shown that nearly all O stars are X-ray emitters, but that only about half of very early B stars and a handful ($\sim 5\%$) of mid- and late-B stars are detectable X-ray sources (Chlebowski, Harnden, & Sciortino 1989; Grillo et al. 1992; Meurs et al. 1992; Berghöfer et al. 1997). While the O stars follow the relation $L_X/L_{Bol} \approx 10^{-7}$ (see, e.g., Pallavicini et al. 1981), B star X-ray luminosities show a lot of scatter (Meurs et al. 1992; Berghöfer et al. 1997). These studies have not been very sensitive, however, with the minimum detectable fluxes typically implying a limiting luminosity of $L_X \approx 10^{30}$ ergs s^{-1}. A much more sensitive survey of 11 early-B V stars was presented by Cassinelli et al. (1994, hereafter Paper I). That study showed that X-ray luminosities decrease rapidly from B0 to B3 and that B V stars have generally softer X-ray spectra than O stars. This result suggests that the low-detection rates of B stars in the all-sky surveys were due to both their short exposure times and the significant interstellar medium (ISM) attenuation toward most B stars.

Although L_X decreases for stars later than B0, it does not decrease as rapidly as would be expected by standard radiation-driven wind theory. It is possible that the theory systematically underestimates the mass-loss rates for B V stars or that some nonwind X-ray production mechanism

takes over from or augments wind shocks as one looks to later B spectral subtypes (Paper I). The X-ray all-sky surveys and subsequent pointed observations show that a few mid- and even late-B stars are relatively strong X-ray sources—conceivably stronger than could be explained by wind shocks. Binarity does not account for the X-ray emission in all of these systems (Berghöfer & Schmitt 1994a), and there is some suggestion that youth is associated with their X-ray activity (Schmitt et al. 1993). Dachs & Hummel (1996) find that many Bp/Ap stars in the young open cluster NGC 2516 are X-ray sources. There are also indications that coronal/chromospheric activity persists to spectral types even earlier than the theoretical cutoff of convective envelopes (Walter et al. 1995; Freire Ferrero et al. 1995).

The X-ray emission from early-type stars is generally observed to be constant in time, although most observations to date have been brief, with long-timescale variability being very poorly sampled if at all. In only two cases (excluding mass transfer binary systems), increases in X-ray luminosity of more than 30% have been detected in normal O and very early B stars: in the O supergiant ζ Ori (Berghöfer & Schmitt 1994b) and in the Be star λ Eri (Smith et al. 1993). The lack of strong X-ray variability among these stars implies that there are many sites of emission in the wind or in coronal structures at any one time. It has been suggested that roughly 1000 separate angular sections of the stellar wind have to be independently undergoing shock activity in order to provide a globally constant X-ray flux in O supergiant data (Feldmeier et al. 1997b).

The purpose of this paper is to define the X-ray properties of B V stars in the region of the H-R diagram where radiation-driven winds are fading and nonwind X-ray activity may be beginning. To do this, we reanalyze the *ROSAT* PSPC observations of the 11 B V stars already presented in Paper I by using a more realistic wind-attenuation model (Cohen et al. 1996), in some cases including additional data obtained since the publication of that paper, and present data on an additional 16 stars. We will use the *ROSAT* data to address the following questions: (1) How do the X-ray properties of very early B stars compare with those of O stars? (2) Can the decrease in X-ray activity between B0 and B3 be understood entirely within the context of radiation-driven wind theory? (3) How does the inclusion of wind attenuation in the X-ray models affect the derived X-ray properties, including L_X/L_{Bol}? (4) How much evidence is there for the magnetic field–related X-ray activity seen in late-type stars and hinted at in a handful of mid- and late-B stars? (5) Do mid-B V stars have a combination of X-ray–producing mechanisms operating? (6) Are the X-ray properties of Be stars and β Cephei variables different from those of normal B V stars?

2. SAMPLE STARS

Our sample contains 27 stars with spectral types between B0 and B7 and luminosity classes V, IV, or III. Near the top of the main sequence, the difference in luminosity between main-sequence stars and giants is less than an order of magnitude. We therefore refer to this range of luminosity class as "near–main-sequence," and to near–main-sequence B stars as "B V" stars. The luminosities of the stars in the sample range from 300 $L_\odot$ to 4×10^4 $L_\odot$, as compared with 4×10^4 $L_\odot$ for μ Col (O9.5 V) and 10^6 $L_\odot$ for ζ Pup. The luminosities of the B V stars are significantly sub-Eddington ($\lesssim$5%), whereas those for O stars can be a significant fraction of the Eddington luminosity ($\lesssim$ 50%). The mass-loss rates of the stars in our samples are predicted to be in the range of a few times 10^{-12} $M_\odot$ yr^{-1} to a few times 10^{-8} $M_\odot$ yr^{-1}, whereas the mass-loss rates of O stars range from about 10^{-7} $M_\odot$ yr^{-1} to more than 10^{-5} $M_\odot$ yr^{-1}. The stars and several of their observed characteristics are listed in Table 1.

It is important that we use as homogeneous and consistent a set of stellar and wind parameters as possible for our sample stars. When making comparisons among the stars, we must be sure that trends of observed X-ray properties with spectral type or individual stellar parameters are real and not due to random or systematic errors in the determination of the stellar properties. It is very difficult to obtain accurate stellar and wind parameters for a large sample of early-type stars. Wind parameters are especially difficult to ascertain for B V stars because the UV lines only weakly manifest the presence of winds, and very uncertain ionization corrections are needed to convert these observational data into mass-loss rates. Therefore, it is imperative that we use consistent methods and sources for determining the values of the stellar parameters, even if this results in less than fully accurate values.

To accomplish this, we take spectral types and luminosity classes from just two sources in the literature (Hiltner, Garrison, & Schild 1969; Lesh 1968). We then use these spectral types to infer effective temperatures, radii, and masses from the calibration of Straizys & Kuriliene (1981). This calibration of stellar properties with spectral type is based on several other calibrations of effective temperature and absolute bolometric magnitudes taken from the literature combined with evolutionary masses. The mass calibration thus derived disagrees by as much as 20% with other calibrations that are based on spectroscopic analysis. However, we have chosen to use the evolutionary masses because the spectroscopic masses are suspect (because of known problems with plane-parallel atmosphere models of hot stars; see, e.g., Vacca, Garmany, & Shull 1996).

From these adopted stellar parameters, we derive the basic wind parameters, $\dot{M}$ and v_∞. These values are calculated using the "cooking formula" of Kudritzki et al. (1989), which includes the finite cone angle effect and is based on the α, k, δ line-force parameterization pioneered by Castor, Abbott, & Klein (1975). We take the values of the three line-force parameters from the tabulation of Abbott (1982). Although these line-force parameters are no longer considered to be very accurate—because of the neglect of X-rays in the nebular approximation used to calculate ionization and excitation conditions—they are the best that are currently available for B V stars. The validity of the wind properties implied by these adopted line-force parameters will be discussed in § 6 in light of the X-ray properties we derive.

As mentioned above, the wind models and the interpretation of observations both have a high degree of uncertainty due to the lack of knowledge about the wind ionization conditions. In the cases where stellar parameters have been assigned via detailed studies, we have compared these values with our adopted ones and generally find good agreement. By determining the stellar parameters in a consistent and uniform way, we can be fairly sure that the *relative* values of the parameters are accurate. The derived stellar and wind parameters for our sample are listed in Table 2.

TABLE 1

SAMPLE STARS

Star	HD Number	Spectral Type[a]	m_V[a]	log N_H[b] (cm^{-2})	$V \sin i$[c] ($km\ s^{-1}$)
τ Sco	149438	B0 V	2.82	20.43, 20.49, 20.05	20
θ Car	93030	B0.5 V	2.76	20.28, 20.10	150
β Cen	122451	B1 III	0.60	19.63, 19.54, 19.52, 18.81	110
ξ^1 CMa	46328	B1 III	4.33	20.15	10
α Vir	116658	B1 IV	0.97	18.83, 18.98, 19.0	135
λ Sco	158926	B1.5 IV	1.61	19.23, 19.89, <19.85	145
δ Lup	136298	B1.5 IV	3.21	20.18, 20.00	225
κ CMa	50013	B1.5 IVe	3.94	<19.03, <18.52	200
η Cen	127972	B1.5 Ve	2.30	20.11, <18.70	345
δ Cen	105435	B2 IVe	2.60	19.20, 19.30	155
γ Lup	138690	B2 IV	2.77	20.23	270
μ Cen	120324	B2 IV–Ve	3.26	20.40, 19.01, 19.30	180
κ Vel	81188	B2 IV–V	2.47	19.95, 20.48	55
β Mus	110879	B2 V	3.05	<19.30	185
α Ara	158427	B2 Ve	2.94	<18.70	315
ζ Cen	121263	B2.5 IV	2.54	19.28	225
ι Lup	125238	B2.5 IV	3.55	<19.30	235
α Pav	193924	B2.5 V	1.93	<19.30	20
α Tel	169467	B3 IV	3.50	<19.30	20
σ Sgr	175191	B3 IV	2.09	19.11	205
α Eri	10144	B3 Ve	0.48	18.78, 19.00, 18.77	250
η Aur	32630	B3 V	3.16	18.84	125
η UMa	120315	B3 V	1.84	17.00, 17.85	195
μ Eri	30211	B4 IV	4.00	<20.00	160
λ CMa	45813	B4 V	4.47	18.41	135
τ Her	147394	B5 IV	3.88	<18.04	30
α Col	37795	B7 IVe	2.63	<18.70	210

[a] From Hiltner et al. 1969, except α Vir, η Aur, η UMa, τ Ori, μ Eri, and τ Her, which are from Lesh 1968. Stars that often have been identified as Be stars in other studies are given the "e" designation, even if neither Hiltner et al. 1969 nor Lesh 1968 identifies them as such.

[b] From Fruscione et al. 1994 and Welsh 1991; the upper limits for β Mus, ι Lup, α Tel, and μ Eri were derived from Figs. 2 and 3 in Welsh et al. 1994.

[c] From Uesugi & Fukuda 1982.

Most of the sample stars are B3 or earlier, with only four stars B4 or later. As we will show, the X-ray properties change significantly between roughly B1 and B3. In order to emphasize this dichotomy, we refer to B0 and B1 stars as "very early B stars" throughout this paper, and stars B3 and later as mid-B. We chose the objects in our sample based primarily on the criterion that the interstellar column densities are very low ($N_H \lesssim 10^{20}$ cm^{-2}, corresponding to an optically thin interstellar sight line above 200 eV). We also took proximity, the existence of a large amount of observational data at other wavelengths, and the need to include several different special categories of stars into account when choosing our sample stars. We must stress that this sample is neither a random magnitude-limited data set nor a volume-limited data set. It contains many of the nearby early- and mid-B V stars, but it excludes many others, mostly, but not exclusively, because of high ISM column densities. However, the sample should be relatively representative because X-ray emission properties were not a criterion for selecting the program stars.

The observational sample includes three special categories of stars: β Cephei variables, Be stars, and stars with anomalous wind properties. There are four β Cephei variables in the sample: α Vir, λ Sco, β Cen, and ξ^1 CMa. The β Cephei variables lie in a strip above the main sequence, extending between spectral subtypes B0 and B3 and luminosity classes V and III. They often show multiple periods, between 4 and 7 hr. Their light curves lag behind their radial velocity curves by a quarter of a period, indicating that they are most luminous when their radii are smallest. This behavior can be explained as a periodic change in effective temperature, typically of a few hundred kelvins (Sterken & Jerzykiewicz 1993). The cause of the pulsation has been identified only recently as the kappa mechanism related to a peak in the iron opacity around 2×10^5 K (Moskalik & Dziembowski 1992; Kiriakidis, El Eid, & Glatzel 1992). Whether X-ray emission in B V stars originates near the photosphere or in the wind, this type of variability might be expected to influence it.

There are seven Be stars in the sample: α Eri, η Cen, κ CMa, δ Cen, α Ara, μ Cen, and α Col. Be stars are B V stars that at one time showed emission in Hα or one of the other Balmer series lines. About 25% of B1 stars are Be stars, with the frequency of Be stars decreasing at both earlier and later spectral subtypes (Briot & Zorec 1994). Observations imply the presence of circumstellar material in Be stars, and the data now indicate overwhelmingly that this material is in a disklike distribution, although the details of the matter distribution and velocity field in the circumstellar material are still not known (Waters & Marlborough 1994; Wood, Bjorkman, & Bjorkman 1997). Many Be stars appear to have episodes of enhanced mass loss and disk activity, including the so-called "shell" stages and possibly one-armed spiral wave structures in the disk (Telting et al. 1994). Some Be stars show evidence of magnetic activity (Smith et al. 1993, 1994). Although there are several competing models of Be stars—including the WCD model in which stellar rotation focuses polar wind material

TABLE 2

SAMPLE STARS: DERIVED QUANTITIES

Star	Spectral Type	$\log L_{Bol}$[a] ($L_\odot$)	T_{eff}[a] (K)	R_*[a] ($R_\odot$)	M_*[a] ($M_\odot$)	$\dot{M}$[b] ($M_\odot$ yr^{-1})	v_∞[b] (km s^{-1})	Distance[c] (pc)
τ Sco	B0 V	4.69	31480	7.24	20.0	3.1×10^{-8}	2400	231
θ Car	B0.5 V	4.45	28870	6.53	16.0	1.2×10^{-8}	2160	200
β Cen	B1 III	4.61	26490	9.33	17.0	2.7×10^{-8}	1640	105
ξ^1 CMa	B1 III	4.61	26490	9.33	17.0	2.7×10^{-8}	1640	583
α Vir	B1 IV	4.41	26490	7.41	15.1	1.0×10^{-8}	1750	94
λ Sco	B1.5 IV	4.21	24690	6.84	12.9	4.2×10^{-9}	1560	105
δ Lup	B1.5 IV	4.21	24690	6.84	12.9	4.2×10^{-9}	1560	220
κ CMa	B1.5 IVe	4.21	24690	6.84	12.9	4.2×10^{-9}	1560	308
η Cen	B1.5 Ve	3.99	24690	5.31	11.2	1.5×10^{-9}	1660	110
δ Cen	B2 IVe	4.01	23010	6.31	9.8	2.0×10^{-9}	1310	138
γ Lup	B2 IV	4.01	23010	6.31	11.0	1.6×10^{-9}	1400	149
μ Cen	B2 IV–Ve	3.89	23010	5.50	10.4	8.5×10^{-10}	1470	163
κ Vel	B2 IV–V	3.89	23010	5.50	10.4	8.5×10^{-10}	1470	113
β Mus	B2 V	3.77	23010	4.79	9.8	4.5×10^{-10}	1540	129
α Ara	B2 Ve	3.77	23010	4.79	9.8	4.5×10^{-10}	1540	122
ζ Cen	B2.5 IV	3.77	21090	5.69	9.2	4.1×10^{-10}	1250	112
ι Lup	B2.5 IV	3.77	21090	5.69	9.2	4.1×10^{-10}	1250	178
α Pav	B2.5 V	3.55	21090	4.42	8.2	1.3×10^{-10}	1360	64
α Tel	B3 IV	3.53	19320	5.13	7.6	1.2×10^{-10}	1220	145
σ Sgr	B3 IV	3.53	19320	5.13	7.6	1.2×10^{-10}	1220	76
α Eri	B3 Ve	3.33	19320	4.07	6.9	4.2×10^{-11}	1330	27
η Aur	B3 V	3.33	19320	4.07	6.9	4.2×10^{-11}	1330	94
η UMa	B3 V	3.33	19320	4.07	6.9	4.2×10^{-11}	1330	51
μ Eri	B4 IV	3.21	17260	4.42	6.3	3.1×10^{-11}	1350	30
λ CMa	B4 V	3.03	17260	3.59	5.8	1.3×10^{-11}	1440	139
τ Her	B5 IV	2.89	15420	3.80	5.2	9.8×10^{-12}	1390	104
α Col	B7 IVe	2.45	12790	3.39	3.7	3.0×10^{-12}	1250	44

[a] The theoretical prediction is based on the spectral type and luminosity class taken from Straizys & Kuriliene 1981.

[b] The values are derived from the line-force tabulation of Abbott 1982, using the "cooking formula" of Kudritzki et al. 1989.

[c] The distance modulus is based on the V magnitude from Hiltner et al. 1969 or Lesh 1968, and the theoretical prediction of M_V is from Straizys & Kuriliene 1981.

to the equatorial regions (Bjorkman & Cassinelli 1993)—there is a consensus that rapid rotation plays some role in generating or sustaining their disks. The possibility of magnetic activity, the concentration of matter into the equatorial plane, and the interaction of the stellar wind and the disk all have implications for the generation of X-ray emission in Be stars.

The sample stars τ Sco, θ Car, and ξ^1 CMa all have stronger winds than other stars of their spectral subtypes. This has been determined from the study of UV line profiles (Walborn, Parker, & Nichols 1995). While ξ^1 CMa is also a β Cephei variable and θ Car is chemically peculiar, τ Sco is unusual in several ways. It shows evidence of redshifted absorption in several high-ion UV lines, possibly indicating the presence of infalling material (Lamers & Rogerson 1978). It may be extremely young, having been determined by Kilian (1992) to have arrived on the main sequence less than one million years ago. It has a very low projected rotational velocity, indicating that it is viewed almost pole-on, and it has several near-infrared Brackett lines in emission, suggesting that it might be a Be star with a weak disk (albeit without Hα in emission) seen pole-on (Waters et al. 1993). Both youth and enhanced wind activity might affect X-ray production. These characteristics will be discussed later in the context of this star's unusual X-ray properties.

Of the 27 B V stars in the sample, observations of 11 of them have been reported on in Paper I. For several of these objects, additional *ROSAT* data have been obtained since then and are included in the analysis presented in this paper. For all of these 11 stars, we have reanalyzed the X-ray spectra using new, more realistic models that will be discussed in § 5. The 16 new stars are primarily of later spectral subtypes (B2–B7).

3. DATA

All of the observations reported in this paper were made with the *ROSAT* PSPC and were obtained as part of NASA's guest observing program, cycles 1–4. Many of the 27 stars were observed more than once, with observations sometimes spanning several years. Details are supplied in Table 3. Note that many of the stars reported on in Paper I have been reobserved since that paper was published.

The *ROSAT* telescope mirrors, in combination with the PSPC instrument, have an on-axis spatial resolution characterized by a FWHM $\approx 25''$. The PSPC is a proportional counter with a spectral resolution of $E/\Delta E = 2.3$ at 0.93 keV that increases with photon energy as $E/\Delta E \propto E^{1/2}$. The sensitivity of the telescope and detector is excellent, with low and well-understood background levels (see Trümper 1983 and Pfeffermann et al. 1986 for descriptions of the telescope and detector).

For observations of three stars (α Vir, β Cen, and η UMa), we used the boron filter on the PSPC. This filter blocks transmission above the K-shell edge of boron at 188 eV. When such observations are combined with unfiltered observations, it effectively divides the softest PSPC band into two sections, increasing the spectral resolution of the instrument.

We performed all of our data reduction with the MIDAS/EXSAS software. Sources were extracted using circular

TABLE 3

ROSAT OBSERVATIONS

Star	Observation Dates	Exposure Time (s)	Counts[a]	Count Rate[a] (counts ks^{-1})
τ Sco[b]	1991 Mar 1–1993 Sep 5	2596	4391.1 ± 69.0	1691.4 ± 26.5
τ Sco[c]	1991 Mar 1–3	891	1469.6 ± 40.4	1649.3 ± 45.3
τ Sco[d]	1993 Sep 3–5	1705	2920.0 ± 56.1	1712.6 ± 32.9
θ Car	1992 Aug 18–19	1504	549.8 ± 24.0	365.5 ± 15.9
β Cen[e]	1992 Jul 23–1993 Jan 29	2863	3071.0 ± 56.0	1072.6 ± 19.5
β Cen[f]	1992 Jul 24–1993 Jan 29	4449	717.8 ± 27.7	161.3 ± 6.2
ξ^1 CMa	1992 Apr 3–5	1991	228.0 ± 17.8	114.5 ± 8.9
α Vir[e]	1992 Jan 20–21	672	722.4 ± 27.6	1074.7 ± 41.2
α Vir[f]	1990 Jul 18–1992 Jan 23	5422	639.8 ± 27.1	118.0 ± 5.0
λ Sco	1991 Feb 26–28	1384	594.5 ± 25.6	429.5 ± 18.4
δ Lup	1993 Aug 28–30	3210	189.3 ± 17.0	8.9 ± 5.2
κ CMa	1992 Oct 29–31	4636	73.4 ± 9.7	5.8 ± 2.0
η Cen	1992 Aug 11–1993 Jan 26	6295	69.4 ± 12.4	11.0 ± 1.9
δ Cen	1993 Jul 13–15	3888	57.2 ± 9.1	14.7 ± 2.3
γ Lup	1992 Aug 26–29	6603	96.5 ± 12.6	14.6 ± 1.9
μ Cen	1993 Aug 17–21	4681	232.5 ± 17.6	9.6 ± 3.7
κ Vel	1993 Jul 9–12	4821	69.5 ± 11.4	14.4 ± 2.3
β Mus	1993 Aug 29–31	3580	2.4 (fixed); <0.67 (free)	<0.67; <0.19
α Ara	1992 Sep 27–29	3789	20.2 ± 6.4	5.3 ± 1.6
ζ Cen	1993 Jul 22–Aug 25	4651	11.3 ± 4.5 (visual); <16.6 (free)	2.4 ± 1.0; <3.65
ι Lup	1993 Aug 12–21	6097	5.1 ± 8.8 (fixed); <3.78 (free)	0.8 ± 1.4; <0.62
α Pav	1991 Mar 24–1993 Oct 10	2230	60.1 ± 10.3	26.9 ± 4.6
α Tel	1992 Oct 7–10	9787	9.9 ± 13.6 (visual); <14.1 (free; 42″)	1.0 ± 1.4; <1.44
σ Sgr	1991 Mar 30–Apr 3	3184	29.4 ± 7.1	9.2 ± 2.2
α Eri	1991 May 7–9	1661	50.6 ± 8.4	30.4 ± 5.0
η Aur	1993 Sep 19–21	5529	13.3 ± 7.4 (visual); <11.67 (free)	2.4 ± 1.3; <2.1
η UMa[e]	1992 May 25–29	2616	9.6 ± 4.4 (visual); <13.08 (free; 56″)	3.6 ± 1.6; <5.0
η UMa[f]	1992 May 27–30	4856	3.9 ± 3.7 (fixed); <3.7 (free)	0.8 ± 0.8; <0.8
μ Eri	1992 Sep 2–5	10056	71 ± 11[g]	7.1 ± 1.1[g]
λ CMa	1993 Oct 28–31	5997	<6.8 (free; 50″)	<1.1
τ Her	1992 Aug 26–28	3905	30.5 ± 9.8	7.8 ± 2.5
α Col	1993 Feb 12–13	8269	53.5 ± 10.7	6.4 ± 1.2

[a] The methods used for determining the upper limits are described in the text. Briefly, "fixed" and "visual" refer to the upper limits determined by fixing the location on the detector of the purported source, whereas "free" refers to the limits determined by a maximum likelihood search of the central region of the detector.

[b] Combined cycle 1 and cycle 3 data sets.

[c] Cycle 1 data.

[d] Cycle 3 data.

[e] Open exposure; boron filter not employed.

[f] Boron filter exposure.

[g] Due to blending with another X-ray source, these are estimates.

regions with radii determined by visual inspection or the radial intensity profiles. When "ghost images" (Nousek & Lesser 1993) were present, we used a source circle large enough to encompass them, usually having a radius of 6′. The background spectra were sampled from annuli surrounding the source-extraction circle, unless other point sources were present in this area. In those cases, we sampled the background from a source-free area near the center of the field.

For stars that were not detected at least at the 3 σ level, we calculated an upper limit to the count rate in two of three different ways. The first is based on the application of the standard extraction procedure using an extraction cell location corresponding to the star's coordinates ("fixed"). The second is similar to the first, but the location of the source extraction cell was chosen based on a visual inspection ("visual"). For both of these methods, we performed a background subtraction, just as we did for the detections, and we list in Table 3 the count rate and 1 σ uncertainty. The third method involves the maximum likelihood estimator implemented in the EXSAS task compute/upper. For this procedure ("free"), we allowed the task to search within 100″ of the center of the detector, unless there are other identified, bright sources nearby, in which case we truncated the search radius to the value indicated in the table.

The source extraction procedure for both detections and nondetections was straightforward to apply to all of the stars except μ Eri. This object presented a difficulty because it lies about 30″ away from a brighter source, causing its detected image in the *ROSAT* PSPC to be blended with the other source. We therefore extracted the μ Eri source counts from a region that we defined by eye. This extraction is probably subject to contamination by photons from the other source, with an estimated 10%–40% of the extracted counts due to this other source. We analyze μ Eri in § 5 with the other detections, but the luminosity and spectral characteristics we derive are subject to larger uncertainty than the other stars. A follow-up observation with the *ROSAT* HRI will be discussed in a future paper.

The time variability of the eight brightest objects in our sample is discussed in Appendix A. As reported there, we find low-level variability in only two of these eight stars and are able to put upper limits of less than 10% on the variability amplitudes of many of the other stars. This lack of dramatic X-ray variability is in line with previous high signal-to-noise ratio observations of O stars and justifies

fitting the complete *ROSAT* data set of each star as a single spectrum.

4. ARE OBSERVED X-RAYS INTRINSIC TO B V STARS?

We must now ask whether all of the observed X-rays really originate on the B V stars or whether it is possible that some of the detections are due to binary companions. Answering this question is not as straightforward as it might seem. It is impossible to rigorously prove that a given star does not have a binary companion, but at the same time much of the data on binarity of early-type stars is suspect because accurate radial velocity determinations are difficult to make for broad-lined stars.

In general, binaries fall into two categories, depending on their separation and method of detection. The binaries with the smallest separations manifest themselves as spectroscopic binaries: the companion is too close to the primary to be visually resolved, but the orbital motion of the primary is dramatic enough to cause detectable periodic variation in the radial velocity of spectral features of the combined spectrum. The binaries with large separations can be detected as visual binaries: they can be resolved spatially in optical observations. In this case, an estimate of the magnitude difference, and sometimes the spectral type of the companion, can be made. In this discussion, it is important to keep in mind that the spatial resolution of *ROSAT* is much poorer than that of optical telescopes, and so a binary system with components that can be visually resolved may be completely unresolved in a *ROSAT* observation. It is also important to keep in mind that triple systems and even systems with more than three gravitationally bound stars are not unknown.

We only have to worry about contamination of the X-ray spectrum by a purported binary companion if the companion is likely to be an X-ray source with a luminosity comparable to that of the primary. Because stars from mid-B to mid-F are not generally strong X-ray sources, we do not need to be concerned about contamination by companions that are only a few magnitudes fainter than the B V stars in question. Such companions may contribute a few percent to the observed X-ray flux, but this will not affect our analysis of the X-rays from the B V star primary. At least four of our sample stars fall into this category: α Vir, β Cen, λ Sco, and σ Sgr all have companions that are nearly as bright as the primaries (Hanbury Brown, Davis, & Allen 1974). There are several others with companions just a few magnitudes fainter than the primaries (Hoffleit & Jaschek 1982). We can assume that in most of these cases, no more than a small fraction of the X-rays detected are due to binary companions.

For close binaries in our sample, we have no evidence of mass transfer–related X-rays, nor is there reason to expect X-rays from wind-wind collisions in B V stars. Several stars in our sample have visual companions with separations greater than 25″, which is the FWHM spatial resolution of the *ROSAT* PSPC. These stars include ξ^1 CMa, δ Cen, μ Cen, α Ara, and α Pav. It is interesting to note that in the case of ξ^1 CMa only, the companion is detected in our *ROSAT* observations. This is an indication that even when companions are known to be present, they very well may not be strong enough X-ray sources to contaminate the B V stars' data.

Thus, many of the sample stars are likely to be uncontaminated by X-ray emission from binary companions, but some undetermined sample members are likely to have X-ray–emitting late-type companions. This leads us to ask the following: what type of binary companions might be likely to lead to contamination of the B V star X-rays? In order to pose a problem, such a companion must have a large enough X-ray flux to compete with the B V star, and it must be spectrally indistinguishable from the B V star. As we discussed above, stars between mid-B and mid-F are unlikely to be bright enough, but how X-ray bright are the late-type dwarfs that have X-ray–emitting coronae? The Sun's quiescent X-ray luminosity is a little over 10^{27} ergs s^{-1} (Haisch & Schmitt 1996), which is negligible compared with all but the very dimmest of the B V stars in our sample. In a reanalysis of *Einstein* observations of late-type dwarfs, Schmitt & Snowden (1990) estimated a mean X-ray luminosity of about 1.5×10^{28} ergs s^{-1}. However, very young stars seem to have higher mean X-ray luminosities (Briceño et al. 1997). There are only about four stars in our sample that are detected at or below a few times 10^{28} ergs s^{-1}. In general, this determination of the mean X-ray luminosity for late-type stars implies that we do not need to worry about contamination in any of the very early B V stars we detect with $L_X \gtrsim 10^{30}$ ergs s^{-1}.

A further indication of contamination of the X-ray spectrum by a binary companion would be the observation of a hard X-ray spectrum. As we show in the next section, B V stars have very soft X-ray spectra (with only a few exceptions). The power-law indices that we fitted are quite negative, whereas the power-law indices fitted to late-type dwarfs are almost always positive, and the maximum temperatures are usually over 10 MK (Schmitt et al. 1990). The isothermal fits we made to our low-count sample stars, listed in Table 7 below, show that with the mild exception of μ Eri, these stars also have very soft X-ray spectra, inconsistent with the much harder spectra of late-type stars and especially of young late-type stars (Briceño et al. 1997). The star μ Eri, as we discussed in § 3, is somewhat contaminated by a bright companion that we were able to separate crudely from the B V star primary. However, it is likely that some of the X-ray counts we extracted are due to the companion, and an analysis of the companion's *ROSAT* spectrum shows that indeed it is much harder than that of μ Eri itself. Therefore, we have most likely overestimated its spectral hardness and temperature.

Another experimental test of the contribution of binary companions to the overall X-ray fluxes of B star binary systems was carried out by Berghöfer & Schmitt (1994a). These authors made follow-up *ROSAT* HRI observations of eight known binary systems with B star primaries that had been detected with the PSPC instrument in the *ROSAT* all-sky survey. These binaries all have separations large enough to be resolved spatially by the HRI but not by the PSPC. In seven of the eight cases, the primary X-ray source proved to be the B star. Even more interesting to note is that in all seven of these cases, the later type companions were not detected at all. This is further evidence that late-type dwarfs that are in binary systems with B stars have relatively low X-ray luminosities.

In summary, although X-ray emission detected from any given B V star may be attributed to a purported binary companion, statistical arguments about the X-ray flux level, the spectral properties, and empirical evidence regarding the likelihood of detecting X-rays from such a companion strongly argue against contamination in most cases. One to

a few of the stars we detect in our sample might have their X-rays attributed to binary companions, but for a large majority of the detections in the sample, most of the X-rays are likely to be intrinsic. We consider that the strongest overall evidence for this is the very soft X-ray spectra of nearly all of the B stars that have fluxes low enough to make contamination a concern.

5. SPECTRAL ANALYSIS

Spectral analysis holds the possibility of diagnosing plasma temperatures, densities, velocity fields, and compositions. However, X-ray spectral analysis is still at a rudimentary stage compared with astronomical spectroscopy in the optical and UV regimes. There are only a handful of independent-resolution elements in *ROSAT* PSPC data, so we must restrict ourselves to simplified models with only a few adjustable parameters. However, we also should make an effort to use the most realistic model possible to fit the data. For both wind shocks and coronal emission mechanisms, one expects to have multiple physical sites of emission that both individually and as a whole have a wide range of densities and temperatures. Because the origin of the X-ray emission of B V stars is not known with a high degree of certainty, it makes sense to forgo spectral models that are based on a detailed description of a specific mechanism. We therefore did not use specific shock models or coronal models to fit the *ROSAT* data. Rather, we fitted an empirical X-ray emission and transfer model and derived values of basic physical quantities that must be reproduced by any detailed model that purports to describe the high-energy processes on OB stars.

In Cohen et al. (1996), we introduced a model based on a continuous temperature distribution, or differential emission measure (DEM). To keep the number of free parameters to a minimum, we assumed $d\mathrm{EM}/dT \propto T^{\alpha}$ over some temperature range. The other component of this model is local attenuation, the form of which depends on the assumed spatial distribution of the hot X-ray–emitting plasma relative to the cold absorbing wind. For the *ROSAT* PSPC data, we used three free parameters to describe the plasma temperature distribution, the power-law index, α, and the minimum and maximum temperatures, $T_{\min}$ and $T_{\max}$. The wind attenuation is completely specified by the assumed mass-loss rate and spatial distribution of the X-ray–emitting plasma from which we calculated a wind ionization distribution. The only other free parameter is the normalization, which is proportional to the total emission measure. This model therefore has no more free parameters than does the common two-temperature model.

These plasma temperature distributions were converted to high-resolution X-ray spectral models using the MeKaL (Mewe, Kaastra, & Liedahl 1995) plasma code. The MeKaL code gives significantly better fits to *ASCA* data of early-type stars than do other, older codes (Cohen, Cassinelli, & Waldron 1997). The abundances of the model plasma are adjustable, and we fixed them at the mean B star values as determined by Geis & Lambert (1992), or at the general cosmic values found by Anders & Grevesse (1989) for elements that have no B star determination (see Table 4). We fixed the electron density at $n = 10^{10}$ cm^{-3}.

To approximate attenuation of X-rays emitted in a plasma distributed uniformly through the absorbing wind starting at some inner radius R_0, we have previously (Cohen et al. 1996) derived a relationship between the observed flux, f_{obs}, and the emitted, or unattenuated, flux, f_{em},

$$f_{\mathrm{obs}} = f_{\mathrm{em}} \frac{R_0}{\max\,[R_0,\, R_1(\lambda)]}\,, \tag{1a}$$

or equivalently,

$$L_{\mathrm{X}}^{0} = L_{\mathrm{X}} \frac{R_0}{\max\,[R_0,\, R_1(\lambda)]}\,, \tag{1b}$$

where R_1 is the radius at which the optical depth is unity, R_0 is the radius beyond which X-ray–emitting plasma is distributed throughout the wind, and L_{X}^{0} is the emergent X-ray luminosity. This is based on the "exospheric" assumption that all of the X-rays generated above the optical depth unity surface are seen, and that all those generated deeper in the wind than R_1 are absorbed (Cohen et al. 1996). We assume a β-velocity law of the form

$$v(r) = v_{\infty}(1 - R_{*}/r)^{\beta}\,, \tag{2}$$

where v_{∞} is the terminal velocity and R_{*} is the radius of the star. This velocity law yields

$$R_1 = R_{*}\left\{1 - \left[1 - \frac{4\pi\mu m_{\mathrm{H}} v_{\infty} R_{*}(1-\beta)}{\sigma_{\lambda}\dot{M}}\right]^{1/(1-\beta)}\right\}^{-1}\,, \tag{3}$$

where σ_{λ} is the cross section per particle. We took $\beta = 0.8$ for all the stars in our sample.

It turns out that wind attenuation of the X-rays is important only for stars earlier than B2, even if all of the X-ray–emitting plasma is in coronal structures near the stellar surface. Being most like O stars, these are the stars in our sample that are most likely to have wind shocks. Therefore, we feel that this empirical wind-shock model, using the exospheric approximation, is justified for the very early B stars, and for the mid-B stars, wind attenuation is unimportant because of the very small expected mass-loss rates. In the case of ϵ CMa (B2 II), Cohen et al. (1996) confirmed that models in which all of the attenuation arises in an overlying

TABLE 4

PLASMA ABUNDANCES USED IN SPECTRAL MODELING

Element	Abundance[a]
He[b]	11.00
C[b]	8.20
N[b]	7.81
O[b]	8.68
Ne[b]	7.97
Na	6.33
Mg	7.58
Al[b]	6.45
Si[b]	7.58
S[b]	7.21
Ar	6.56
Ca	6.36
Fe[b]	7.72
Ni	6.25

[a] Abundance by number, expressed logarithmically with respect to hydrogen, where $X_{\mathrm{H}} = 12.00$.

[b] These elements are from Geis & Lambert 1992; the others are from Anders & Grevesse 1989.

slab (and thus with attenuation of the form $e^{-\tau}$) cannot fit the *EUVE* and *ROSAT* data from this star; only models using the exospheric approximation gave good fits.

To implement the wind attenuation component of our X-ray spectral model, we had to make an assumption about the stars' mass-loss rates. As we described in § 1, the mass-loss rates of B V stars are very poorly known. So for each star with a high-count spectrum, we fitted the data three times, once with the mass-loss rate and terminal velocity given by the application of the modified wind theory (mCAK) using the α, k, and δ parameters of Abbott (1982) and the Kudritzki et al. (1989) cooking formula, and two additional times: once with 3 times the theoretical value of $\dot{M}/v_\infty$ and once with $\frac{1}{3}$ the value. We calculated the ionization balance in the absorbing wind material using our non-LTE statistical equilibrium and radiation transfer wind code described in MacFarlane et al. (1994). This code accounts for the photoionization by the X-ray radiation field. The wind temperature structure is adapted from the results of Drew (1989). This code is too time consuming to be used directly for model fitting. However, because the X-ray spectrum is an input to the wind ionization routine, we performed an iterative process in which each successive ionization balance was calculated using an updated input X-ray spectrum. We first fitted the *ROSAT* data assuming no wind attenuation. Then the best-fit model we derived was used as input to the wind ionization code, and the ionization balance in the wind was determined. Using this ionization balance, we refitted the *ROSAT* data assuming that wind attenuation is important. This led to a new best-fit X-ray spectral model that was used as input to the wind ionization code, and the procedure was repeated. Usually only 2 or 3 cycles were needed to achieve convergence. The ionization balance thus derived for each $\dot{M}/v_\infty$ case for each star was then combined with the bound-free cross sections of each ion to give the mean energy-dependent cross section per particle used in equation (3). We used the atomic cross sections calculated by Wang, Cohen, & MacFarlane (1997).

Interstellar attenuation was accounted for by using the cross sections of Morrison & McCammon (1983) for a neutral, cosmically abundant gas. We used the hydrogen column densities determined from optical and/or UV spectroscopy for each star listed in Table 1. The model X-ray spectra, f_λ, were then given by

$$f_\lambda = \frac{L_\lambda}{4\pi D^2}\, e^{-\tau_{\rm ism}} \tag{4}$$

and

$$L_\lambda = \frac{R_0}{\max\,[R_0,\, R_1(\lambda)]}\, {\rm EM_X}\, k \int_{T_{\rm min}}^{T_{\rm max}} T^\alpha \Lambda(T,\, \lambda) dT\ , \tag{5}$$

where k is a normalization constant and $\rm EM_X$ is the emission measure. We took $R_0 = 1.5R_*$, which is roughly consistent with numerical simulations (Cooper 1994; Feldmeier 1995). For those stars having observations with more than a hundred total counts, we fitted this model, allowing the emission measure, $\rm EM_X$, and the plasma temperature distribution parameters α, $T_{\rm min}$, and $T_{\rm max}$ to be free parameters. We note that even if we have overestimated R_0, the effect on our derived fits will not be drastic. If X-ray production begins at $1.2R_*$, rather than $1.5R_*$, the wind column density will increase only by about 50%.

We binned the PSPC pulse-height data so that there were at least 10 counts per bin, in order to be able to use the χ^2 statistic as the goodness of fit indicator. We fitted the models given by equation (5) and used the $\Delta\chi^2$ criterion for joint probability distributions (Lampton, Margon, & Bowyer 1976) to determine the confidence limits of each parameter. The best-fit model parameters and the 90% confidence limits are listed in Table 5 for the eight stars to which the power-law emission plus wind attenuation models were fitted. We list the fitted parameters for the models having the theoretical values of $\dot{M}$ and v_∞ for each star. For τ Sco and ξ^1 CMa, we also list the fitted parameters for the case with 3 times the theoretical $\dot{M}/v_\infty$ values.

In Figure 1, we show several of the *ROSAT* PSPC pulse-height spectra, including both the boron filtered and unfiltered (open) observations of β Cen. We also show the hardest and most anomalous spectrum in our sample, that of τ Sco in this figure. For one star, λ Sco, we also show the best-fit model before convolving it with the instrumental response matrix in order to demonstrate the large number of emission lines in the intrinsic spectrum (and the overwhelming smoothing effect of the detector).

TABLE 5

PARAMETER VALUES FROM DIFFERENTIAL EMISSION MEASURE MODEL FITTING

Star	Spectral Type	χ^2_ν	N	log $T_{\rm min}$[a,b] Value (K)	log $T_{\rm min}$[a,b] Range (K)	log $T_{\rm max}$[a,b] Value (K)	log $T_{\rm max}$[a,b] Range (K)	α[a] Value	α[a] Range	log EM[a] Value ($\rm cm^{-3}$)	log EM[a] Range ($\rm cm^{-3}$)
τ Sco.....	B0 V	1.3	26	6.35	6.35 to 6.35	7.70	7.45 to 7.70	−1.69	−1.77 to −1.59	54.76	54.74 to 54.77
τ Sco[c].....	B0 V	1.0	26	6.30	6.25 to 6.30	7.70	7.40 to 7.70	−1.70	−1.78 to −1.46	54.79	54.78 to 54.82
θ Car	B0.5 V	1.9	10	6.20	6.05 to 6.25	7.70	6.70 to 7.70	−3.01	−3.90 to −1.34	53.91	53.88 to 53.93
β Cen	B1 III	1.6	31	5.65	5.65 to 5.75	7.00	6.90 to 7.35	−1.79	−1.94 to −1.67	53.77	53.71 to 53.82
ξ^1 CMa	B1 III	4.2	13	6.35	6.30 to 6.35	7.70	7.15 to 7.70	−2.18	−2.41 to −1.76	54.30	54.27 to 54.32
ξ^1 CMa[c].....	B1 III	1.5	13	6.15	6.10 to 6.25	7.70	7.25 to 7.70	−1.86	−2.12 to −1.72	54.44	54.41 to 54.45
α Vir	B1 IV	3.7	18	5.60	5.60 to 5.70	6.80	6.65 to 7.10	−2.16	−2.44 to −1.89	53.16	53.07 to 53.18
λ Sco	B1.5 IV	1.5	8	5.60	5.60 to 5.95	6.50	6.40 to 7.70	−1.48	−3.32 to −0.28	53.39	53.24 to 53.51
δ Lup	B1.5 IV	1.6	6	5.60	5.60 to 6.10	7.30	6.90 to 7.70	−1.35	−1.95 to −0.96	53.31	53.12 to 53.39
μ Cen	B2 IV–Ve	1.7	9	5.60	5.60 to 6.20	7.30	7.00 to 7.60	−0.85	−1.44 to −0.56	52.84	52.73 to 52.93

[a] For each of the four adjustable parameters, the first column lists the value that leads to the best-fit model, and the second column lists the range of the 90% confidence limits.

[b] Because *ROSAT* is sensitive to gas with temperatures on a finite range only, we have not allowed log $T_{\rm min} < 5.6$ or log $T_{\rm max} > 7.7$.

[c] Models with $\dot{M}/v_\infty$ having 3 times the theoretical value. For these two stars, these models are considered to be the best fit.

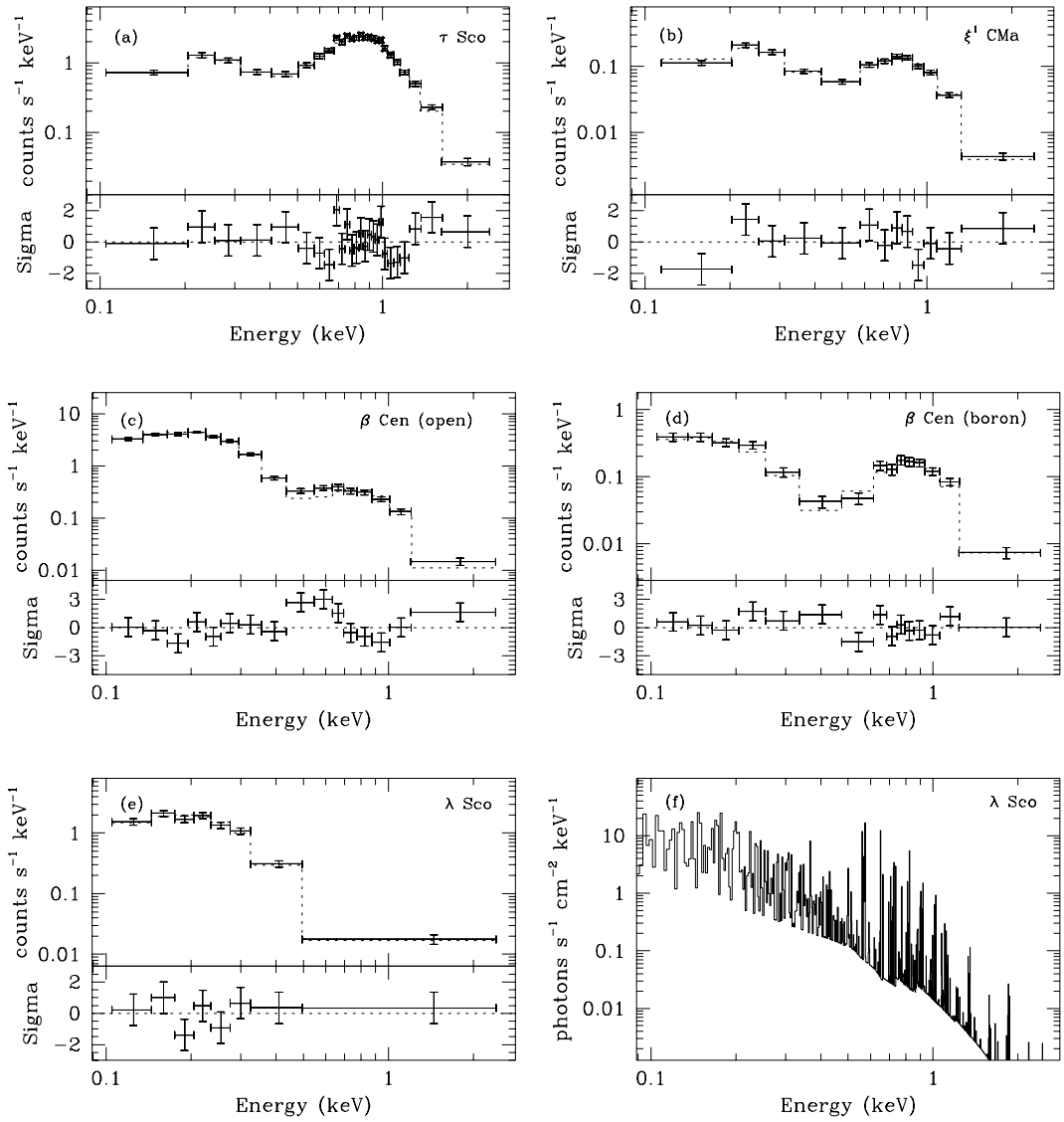

FIG. 1.—Five *ROSAT* PSPC spectra of four stars: τ Sco (*a*), ξ^1 CMa (*b*), β Cen with (*c*) and without (*d*) the boron filter, and λ Sco (*e*). The λ Sco and β Cen data are rather typical, whereas the τ Sco spectrum is by far the hardest in the sample, and the spectrum of ξ^1 CMa is intermediate in spectral hardness. The best-fit models are shown along with the data; below that, the residuals from the model fit are shown. Note that the photon energy labels on the X-axes are only approximate, because of the poor spectral resolution of the PSPC instrument. For λ Sco, we also show the best-fit model before it is convolved with the detector response matrix (*f*). Note the large number of emission lines.

Because the *ROSAT* spectral resolution is so limited, the total X-ray flux is model dependent, and we therefore calculated it on the photon energy range 0.1–2.4 keV from the best-fit models. In Table 6, we list these luminosities, along with the ratio L_X/L_{Bol}, which has been found to be about 10^{-7} for O stars (Pallavicini et al. 1981). Besides the emergent luminosities derived from the model fitting, for those stars with optically thick winds, we also list the total generated luminosities. For three of the eight stars for which we performed spectral fitting, there is wind attenuation in the best-fit models. For several more stars, wind attenuation is important if the mass-loss rates are underestimated. For the 19 stars without enough counts to warrant detailed spectral fitting, we have calculated the X-ray luminosities and upper limits from the *ROSAT* count rates. In order to convert from count rate to flux, we assumed that each star has a plasma DEM characterized by the parameters $\alpha = -2.5$, $\log T_{min} = 5.8$, and $\log T_{max} = 7.2$. The conversion factor then varied between 3.9×10^{-12} ergs cm^{-2} count^{-1} and 16.8×10^{-12} ergs cm^{-2} count^{-1}, depending on the value of the interstellar column density.

In order to get a rough idea of the spectral properties—and hence the plasma temperature distribution—of the stars with a smaller number of total counts, we fitted these data sets with isothermal Raymond & Smith (1977) models. We list the resulting temperatures in Table 7. It should be noted that these temperatures are simply crude indications of the true differential emission measures. Note that we also list these best-fit temperatures for the eight stars that we fitted with DEM models. These can be used as a guide to interpreting the range of DEM model parameters implied by a given value of the isothermal temperature. For example, α Pav and θ Car both have isothermal fits with $T = 2.7 \times 10^6$ K, so we can assume that α Pav has an X-ray spectrum that could be fitted with a DEM model similar to that which fits θ Car. Note that for the eight high-count

TABLE 6

X-RAY LUMINOSITIES

Star	Spectral Type	L_X (ergs s^{-1})	L_X^0 [a] (ergs s^{-1})	log (L_X/L_{Bol})	log (L_X^0/L_{Bol})[a]	log EM (cm^{-3})	ff[b]
τ Sco.....	B0 V	2.01×10^{32}	1.72×10^{32}	−5.97	−6.04	54.76	1.8
τ Sco[c].....	B0 V	2.24×10^{32}	1.45×10^{32}	−5.92	−6.11	54.79	0.18
θ Car	B0.5 V	4.80×10^{31}	4.80×10^{31}	−6.34	−6.34	53.91	1.8
β Cen	B1 III	3.11×10^{31}	1.54×10^{31}	−6.70	−7.00	53.77	0.15
ξ^1 CMa	B1 III	7.38×10^{31}	7.36×10^{31}	−6.33	−6.34	54.44	0.50
ξ^1 CMa[c].....	B1 III	1.13×10^{32}	6.14×10^{31}	−6.14	−6.40	54.45	0.07
α Vir	B1 IV	7.36×10^{30}	7.36×10^{30}	−7.12	−7.12	53.06	0.24
λ Sco	B1.5 IV	1.11×10^{31}	1.11×10^{31}	−6.74	−6.74	53.39	1.5
δ Lup.....	B1.5 IV	9.52×10^{30}	9.52×10^{30}	−6.81	−6.81	53.31	1.2
κ CMa	B1.5 IVe	7.00×10^{29}	...	−7.94	...	52.60	0.24
η Cen	B1.5 Ve	1.41×10^{29}	...	−8.42	...	51.90	0.33
δ Cen	B2 IVe	1.05×10^{29}	...	−8.57	...	51.77	0.10
γ Lup	B2 IV	4.82×10^{29}	...	−7.91	...	52.43	0.83
μ Cen	B2 IV–Ve	2.89×10^{30}	2.89×10^{30}	−7.01	−7.01	52.83	7.1
κ Vel.....	B2 IV–V	2.76×10^{29}	...	−8.03	...	52.19	1.6
β Mus	B2 V	$<5.39 \times 10^{27}$	...	<-9.62	...	<50.48	<0.11
α Ara	B2 Ve	3.75×10^{28}	...	−8.78	...	51.33	0.76
ζ Cen	B2.5 IV	$<2.26 \times 10^{28}$	...	<-9.00	...	<51.10	<0.43
ι Lup	B2.5 IV	$<9.51 \times 10^{27}$	...	<-9.37	...	<50.73	<0.66
α Pav	B2.5 V	5.31×10^{28}	...	−8.41	...	51.48	9.3
α Tel	B3 IV	$<1.46 \times 10^{28}$	...	<-8.94	...	<50.92	<2.8
σ Sgr.....	B3 IV	2.50×10^{28}	...	−8.71	...	51.15	4.8
α Eri	B3 Ve	1.05×10^{28}	...	−8.89	...	50.77	15
η Aur	B3 V	$<8.69 \times 10^{27}$	...	<-8.97	...	<50.69	<13
η UMa	B3 V	$<5.93 \times 10^{27}$	...	<-9.14	...	<50.52	<8.7
μ Eri	B4 IV	6.70×10^{27}	...	−8.96	...	50.58	20
λ CMa.....	B4 V	$<9.97 \times 10^{27}$	...	<-8.61	...	<50.75	<160
τ Her	B5 IV	3.89×10^{28}	...	−7.88	...	51.34	1100
α Col	B7 IVe	5.58×10^{27}	...	−8.28	...	50.50	1200

[a] No value indicates that the wind attenuation is negligible and $L_X = L_X^0$.

[b] The wind filling factor, defined as EM_X/EM_{wind}, using the theoretical $\dot{M}/v_\infty$ for all of the stars.

[c] Models with $\dot{M}/v_\infty$ having 3 times the theoretical value. For these two stars, these models are considered the best fit.

stars, the best-fit χ^2 values in these isothermal models are not acceptable. Additionally, we could not fit the α Ara data because it only contains 20 counts.

Let us briefly summarize some of the trends seen in the data. The quality of the fits have improved compared with the one- and two-temperature fits reported in Paper I. The only ones that we report on here that are not strictly acceptable according to statistical criteria are the fits to α Vir and ξ^1 CMa. In the case of α Vir, this is probably due to systematic uncertainties in the relative calibration of the boron filter detector response matrix and the detector response matrix for the unfiltered configuration. For ξ^1 CMa, we obtain a much better fit when we use a model having 3 times the theoretical $\dot{M}/v_\infty$ value. For this reason, we consider this higher wind density model to be the best fit for ξ^1 CMa. We assume the same for τ Sco. These two stars are seen to have stronger UV wind features than other similar stars (Walborn et al. 1995), and so assuming a higher wind density is reasonable.

TABLE 7

PARAMETER VALUES FROM ISOTHERMAL MODEL FITTING

Star	Spectral Type	T (MK)	χ^2_ν	N
τ Sco.....	B0 V	8.0	8.2	26
θ Car	B0.5 V	2.7	3.5	10
β Cen	B1 III	2.3	6.9	16
ξ^1 CMa.....	B1 III	4.6	2.4	8
α Vir	B1 IV	1.9	3.9	8
λ Sco.....	B1.5 IV	1.7	2.0	8
δ Lup	B1.5 IV	2.8	3.9	6
κ CMa.....	B1.5 IVe	2.9	0.9	5
η Cen	B1.5 Ve	2.9	1.0	4
δ Cen	B2 IVe	2.6	0.1	4
γ Lup	B2 IV	2.1	2.5	5
μ Cen	B2 IV–Ve	4.1	3.3	9
κ Vel.....	B2 IV–V	0.3	2.6	4
α Pav	B2.5 V	2.7	2.7	4
σ Sgr.....	B3 IV	1.3	1.2	3
α Eri	B3 Ve	2.0	1.7	4
μ Eri	B4 IV	5.1	0.1	5
τ Her	B5 IV	2.7	0.5	3
α Col.....	B7 IVe	1.6	0.4	4

The most notable result is the high-detection rate of X-ray sources among the program stars. To assess the change in X-ray luminosity with decreasing stellar effective temperature, we show the ratio of X-ray luminosity to bolometric luminosity plotted against spectral subtype in Figure 2. In the cases of the three stars for which wind attenuation is important, we show both the emergent and generated L_X values. It can be seen that L_X/L_{Bol} declines precipitously from above the canonical O star value of 10^{-7} at B0 to 2 orders of magnitude lower at B2. It then levels off beyond B2, although it is difficult to quantify because of the nondetections between B2 and B3. It is also difficult to draw conclusions about the late-B stars because we have only two stars in our sample with spectral type B5 or later, although both of these are detected. If one accounts for wind attenuation, then the generated X-ray luminosities among the very early B V stars approach $10^{-6} L_{Bol}$. For the even denser winds of O stars, the generated luminosities would be expected to be even larger. It seems that the

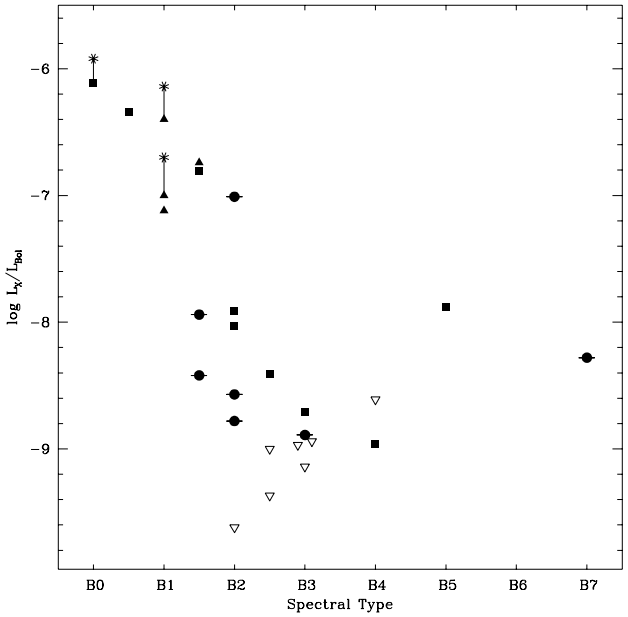

FIG. 2.—The ratio L_X/L_{Bol} for each of the 20 program stars that were detected above the 3 σ level. For three stars, τ Sco, β Cen, and ξ^1 CMa, we indicate the total generated luminosities with asterisks, which are connected to the points, representing the emergent X-ray luminosities, by a line. The upper limits (3 σ) for seven stars are indicated with open triangles. Be stars are indicated by filled circles with lines, and β Cephei variables by filled triangles.

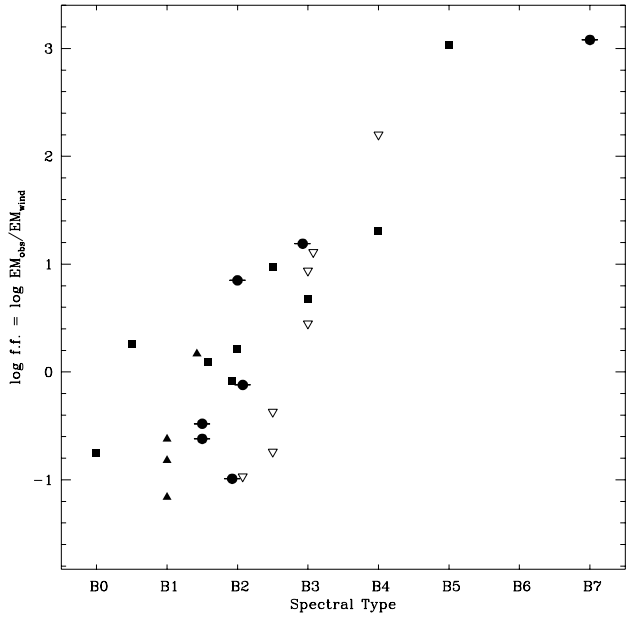

FIG. 3.—The wind filling factors for each of the 20 program stars that were detected above the 3 σ level. The upper limits for seven additional stars are indicated with open triangles. Be stars are indicated by filled circles with lines, and β Cephei variables by filled triangles.

$L_X/L_{Bol} \approx 10^{-7}$ law is, to some extent, an artifact of the traditional neglect of wind attenuation of the X-rays.

We do not show formal error bars on the L_X/L_{Bol} values in Figure 2. The formal statistical uncertainties (90% confidence limits) from the DEM model fitting are typically 10%. Uncertainties in the plasma codes are an additional source of error, but by far the largest source of error on these values is the uncertainty in the bolometric luminosity, which we estimate from the spectral types. These values are only accurate to perhaps 50%, but because we calculated them the same way for each star, we can assume that relative errors in the L_X/L_{Bol} values are significantly less than this. An additional source of uncertainty in the stars with optically thick winds is the total wind attenuation.

Another way to quantify the results of the spectral analysis, and specifically of the derived emission measures, is to calculate the wind filling factor and examine the trends in this quantity versus spectral subtype. We define an emission measure filling factor, $ff = EM_X/EM_{wind}$, where EM_X is the observed X-ray emission measure and EM_{wind} is the total emission measure of the entire stellar wind above $r = R_0$. This analysis assumes, of course, that the X-rays are formed in the stellar wind. If the wind is smooth and spherically symmetrical, it is straightforward to calculate the total emission measure available from wind material above a given radius. Based on the results of numerical simulations (Cooper 1994; Feldmeier 1995), we take that point to be $1.5R_*$, as discussed earlier. We further assume that the wind velocity field is given by a β-velocity law with $\beta = 0.8$ and use the values of the mass-loss rate and terminal velocity given in Table 2. We note that if $R_0 = 1.2R_*$ rather than $1.5R_*$, we will have overestimated the wind filling factors by a factor of 2. We also note that the filling factor has been defined differently by other authors (Hillier et al. 1993; Kudritzki et al. 1996; Feldmeier et al. 1997a). In Figure 3, we show the filling factors and upper limits for the program stars as a function of spectral subtype. These values obviously increase—to well above unity—with decreasing stellar effective temperature. In § 6, we discuss some factors that may mitigate this paradoxical result and draw some conclusions about the applicability of the wind-shock model of OB star X-ray emission.

6. DISCUSSION

The most interesting result of this *ROSAT* survey of 27 B V stars is the high-detection rate. In contrast to the *ROSAT* (Meurs et al. 1992; Berghöfer et al. 1997) and *Einstein* (Grillo et al. 1992) all-sky surveys in which only 5%–10% of the B stars were detected, we detect 20 out of 27 B V stars, for a rate of nearly 75%. Our much different results were obtained for two reasons: the longer observations of nearby stars in our study provided a typical detection threshold that is almost 2 orders of magnitude below those of the surveys, and we chose stars that had very low interstellar column densities. This last point is especially important for B V stars, as opposed to O stars, because the very soft B V star X-ray spectra are especially prone to attenuation by the interstellar medium. The high-detection rate continues beyond the early-B V stars we observed in Paper I and extends to B7.

Because L_{Bol} decreases, the overall X-ray flux levels of B stars decrease as one looks to later spectral subtypes. But in fact we find they decrease much faster than the $L_X/L_{Bol} \approx 10^{-7}$ relation dictates, as Figure 2 shows. However, the decline may level off beyond about B2, with the 11 detected stars later than B1.5 having a mean L_X/L_{Bol} of roughly $10^{-8.5}$. The presence of seven upper limits makes an interpretation of the X-ray luminosity function for the mid-B V stars difficult. It is clear, however, that there is a very wide range of luminosities, since a handful of mid- and late-B stars in other studies have L_X/L_{Bol} values as high as 10^{-5}

(Schmitt et al. 1993; Berghöfer & Schmitt 1994a). It remains to be seen whether some of the nondetected stars in these surveys truly have negligible X-ray emission or whether they have $L_X \lesssim 10^{27}$ ergs s^{-1}, which is below our detection threshold. Three of the "undetected" stars in our sample, ζ Cen, η Aur, and η UMa, are in fact detected at the 2 σ level, so perhaps deeper observations will reveal that most if not all B V stars are X-ray sources.

Figure 3 shows that the wind filling factor increases rather steeply. Among the very early B V stars, the filling factors are roughly 10%. This is significantly more than has been determined for several O stars (Kudritzki et al. 1996; Feldmeier et al. 1997a). Filling factors appropriate to the line-force instability mechanism could be reconciled with our observations if the stars' mass-loss rates are a few times larger than current theoretical calculations predict. This finding is similar to that for the B2 II star ϵ CMa (Cohen et al. 1996).

The very high filling factors (of 10 or more) seen in the stars later than B2 present serious difficulties for explanations in terms of the line-force instability mechanism in the context of radiation-driven winds with reasonable mass-loss rates. Calculations predict that the line-force instability mechanism leads to low-density material being accelerated into reverse shocks and filling factors of no more than 1% (Cooper 1994; Feldmeier et al. 1997a). Perhaps improvements to the treatment of radiative cooling and the extension of the models to two dimensions, rather than the spherically symmetric one-dimensional simulations, may eventually modify this stringent requirement. It is not yet clear whether shell mergers farther out in the flow, as described by Feldmeier et al. (1997b) for O supergiants, could lead to larger filling factors. There is a general limit, however, to the filling factor of shocked gas in a line-driven wind, because if the bulk of the wind is hot and highly ionized, then the wind material lacks the line opacity to provide for radiative driving by the photospheric radiation field. A filling factor of roughly 10 could be generated if 1/10 of the wind were to be compressed by a factor of 100 and heated to temperatures in excess of 0.5×10^6 K. This seems excessive, and it seems clear that some nonwind-shock mechanism must be invoked to explain the X-rays observed in at least some mid- and late-B stars.

If wind shocks can be ruled out, then one is left with magnetic/coronal mechanisms. Unfortunately, no direct evidence for the existence of magnetic fields and coronae on B V stars exists. It has been suggested—again because of X-ray detections of A and B stars—that young B stars may retain a portion of their natal magnetic fields (Schmitt et al. 1993), and furthermore that differential rotation may lead to the formation of a corona in hot stars (Tout & Pringle 1995).

If there was a reliable way to determine the ages of a large sample of B V stars, then it might be possible to determine if there is a correlation between age and X-ray properties. There are some indications that this might be the case. The four young B stars (they are members of binary systems in which the companion has not yet descended to the main sequence) detected with *ROSAT* by Schmitt et al. (1993) all have L_X/L_{Bol} values significantly higher than we find for B V stars later than B1.5. Also, τ Sco, which has the largest L_X/L_{Bol} of any of our sample stars, has been determined to have arrived on the zero-age main sequence less than 10^6 years ago (Kilian 1992). Furthermore, late-B stars that are known to have strong magnetic fields—namely, Bp/Ap stars—in the young cluster NGC 2516 have been found recently to be moderately strong X-ray sources (Dachs & Hummel 1996). These two pieces of evidence suggest that a magnetic/coronal explanation might be a fruitful avenue to explore for mid- and late-B stars.

Additional evidence for coronal activity might come from spectral information. The coronae of K and M dwarfs are quite hard, with temperatures typically over 10^7 K or, alternately, positive power-law slopes in the differential emission measure (Schmitt et al. 1990). Giants to the left of the "dividing line" near early K giants in the H-R diagram also have hard X-ray spectra, as do some active G and F dwarfs (Ayers et al. 1981; Haisch & Simon 1982). Giants to the right of the dividing line do not show X-ray emission, but G and F dwarfs (like the Sun) have quiescent X-ray spectra that are quite soft, implying temperatures of only a few million kelvins (Haisch & Schmitt 1996). Very few of the stars in our sample have spectra hard enough to be comparable to the coronal emission of K and M dwarf stellar coronae. However, because the coronae of B stars would not be produced by deep outer convective zones like the coronae on late-type stars are, it is by no means certain that they would have similar temperature distributions.

The plasma DEMs we derived are weighted strongly to lower temperatures. The power-law indices we found for the differential emission measure model are all consistent with values of α between -1.9 and -1.75, with the exception of μ Cen. Most of the T_{max} values are high ($T \gtrsim 10^7$ K), but this is probably unphysical. *ROSAT* is not very sensitive to gas with temperatures above 10 MK, and because the DEMs are strongly skewed toward cooler gas, even models with $T_{max} = 10^{7.7}$ K may have only negligible amounts of such hot plasma. For most of the stars, the lower temperature bounds are also poorly constrained since *ROSAT* is insensitive to plasma with $T_{min} \lesssim 10^{5.6}$ K. In any case, the differential emission measures we derived are weighted strongly to lower temperatures. This puts the X-ray spectra of these B V stars in relatively good agreement with the predictions of the line-force instability wind simulations (Cooper 1994; Cohen et al. 1996), which show a lot of cooler ($T \approx 10^6$ K) plasma as compared with very hot ($T \approx 10^7$ K) plasma.

It is difficult to compare our results for B V stars with the results of X-ray spectral fitting of O stars because other investigators use different types of models. Upon inspection, O star spectra look harder than B V star spectra (see, e.g., Kudritzki et al. 1996). The canonical early-O star ζ Pup has a relatively hard *ROSAT* spectrum that is fitted by a two-temperature wind emission model that includes wind attenuation (Hillier et al. 1993). The two temperatures, however, are only 1.6 and 5 MK, with nearly equal emission measures for the two components. The two temperatures are low, despite the hard spectrum due to the wind attenuation of (predominantly soft) X-ray photons (Hillier et al. 1993). This plasma temperature distribution may be comparable to the DEMs we derive for most of the very early B V stars, but it is hotter than the isothermal models fit to the mid- and late-B V stars. Some O supergiants, however, have significantly harder X-ray spectra than ζ Pup or any of our sample of B V stars, with the exception of τ Sco. For example, Cassinelli & Swank (1983) used *Einstein* SSS data to ascertain the presence of $T > 10^7$ K gas on ζ Ori A (O9.5 Ia).

The hottest star in our sample, τ Sco, seems to be an exception to many of the generalizations we have made about the B V stars. It has an unusually large X-ray luminosity of $L_X = 2.2 \times 10^{32}$ ergs s^{-1}, and clearly it has the hardest spectrum (see Fig. 1). Recently, Cohen et al. (1997) have used *ASCA* observations to determine that a significant quantity of very hot ($T \gtrsim 25$ MK) plasma exists on τ Sco. The DEM power-law slope we derive in this paper is quite negative, although the 90% lower confidence limit for the slope is higher than for any of the other stars, except μ Cen. The *ASCA* results therefore imply that this decrease in the DEM as a function of temperature levels off above about 10^7 K. Its wind filling factor, while large, is not as large as some of the other stars' wind filling factors, but that is only because the mass-loss rate of τ Sco is quite high for a B V star. To the extent that wind shocks have difficulty explaining the τ Sco data, this star may be linked with the mid- and late-B V stars that have too much X-ray emission to be understood in terms of wind shocks.

Two other stars in our sample, μ Cen and ξ^1 CMa, also have harder X-ray spectra than the rest of the sample: μ Cen is a Be star and is one of the two stars in our sample that shows time variability; ξ^1 CMa is a β Cephei variable, but its spectrum is harder and stronger than those of the other three β Cephei variables in the sample. Perhaps these two stars represent intermediate cases between the extreme properties of τ Sco and the softer, less intense X-ray emission of the bulk of B V stars.

The spectral models we employed include wind attenuation. In three cases—τ Sco, ξ^1 CMa, and β Cen—wind attenuation is expected, based on the theoretical mass-loss rates. And in several others, wind attenuation is important if the mass-loss rates are larger than theory predicts. The primary result of the inclusion of wind attenuation is that the total X-ray luminosity generated in the wind does not escape. In Table 6 and Figure 2, we show for the three relevant stars the adjustments to the L_X/L_{Bol} values that are caused by including wind attenuation. One can only assume that this correction is larger still for the O stars because of their denser winds. Taking this into account, it becomes apparent that the $L_X/L_{Bol} \approx 10^{-7}$ law is an artifact of the neglect of wind attenuation—using our notation, it should be stated as $L_X^0/L_{Bol} \approx 10^{-7}$. It seems that the increased emission that occurs as one goes to earlier spectral subtypes is canceled relatively efficiently by increased attenuation, leading to a basically constant ratio of the *emergent* X-ray luminosity to the bolometric luminosity. Understood in this context, it is reasonable to assume that the $L_X^0/L_{Bol} \approx 10^{-7}$ relationship breaks down at about B1, just where the winds become completely optically thin to X-rays.

The plasma temperature distributions we derive are also somewhat affected by the degree of wind attenuation. Because the energy dependence of the bound-free cross sections is such that the K-shell cross section of each ion is greatest at the threshold energy and decreases sharply beyond that, wind attenuation preferentially affects soft X-rays. When there is more wind absorption, the intrinsic spectrum must be softer as well as brighter in order to offset the increased attenuation of soft X-ray photons. We do find more negative α-values in the cases where we increased the mass-loss rate by a factor of 3, and more positive values in the cases where we decreased the mass-loss rate. The wind ionization conditions we derived in these alternate cases were also somewhat different. In some cases, however, the changes in the ionization balance were mitigated by the fact that increased wind densities lead both to enhanced recombination through the n^2-dependence of this process and to greater ionization due to the need for a brighter and softer input X-ray spectrum. In any case, among our sample stars, the ionization fraction of He II ranges from 1% to 20% (He III is always dominant), and the dominant ionization stage of carbon, for example, ranges from C III to C V.

We have some additional information available to us that may help to constrain further the X-ray production mechanism in both the very early B V stars and the later B V stars. The time constancy that we found in the analysis mentioned in § 3 and described in Appendix A places some further constraints on wind-shock explanations of X-ray production in the B0 and B1 stars. The upper limits, as well as the two detections, of variability amplitudes of roughly 10%–20% are in disagreement with the numerical simulations of line-force instability wind shocks. In these simulations, the X-ray emission is dominated by a few shocks that evolve quite rapidly, leading to variability of an order of magnitude or more on timescales of roughly 10^3 s (Cooper 1994). Of course, the simulations to date have been one-dimensional, spherically symmetric, so that all shock zones are shells that subtend the full 4π steradians. This severely limits the total number of individual shocks that can exist in the wind at any one time. It is quite conceivable that full three-dimensional models could show much less variability as perhaps hundreds of individual shocks contribute to the stellar X-ray emission.

As mentioned in § 1, spherically symmetric wind models have enjoyed a lot of success in explaining the mean properties of O star winds. However, there are both observational and theoretical reasons to believe that many stellar winds are not truly spherically symmetric. Be stars have geometrically thin, dense equatorial disks (Wood et al. 1997), and some OB stars have line profiles that require two component wind models to fit the data (Bjorkman et al. 1994; Prinja et al. 1997). Theoretical calculations show that equatorial density enhancements are expected in many rapidly rotating stars besides Be stars (Ignace, Cassinelli, & Bjorkman 1996). Furthermore, temperature differences across the stellar disk have been shown to lead to different mass-loss properties in different locations in a given stellar wind (Cranmer & Owocki 1996).

While it is true that equatorial compression, or in fact any density enhancement, will provide for more possible emission measure than in an equivalent spherically symmetric wind, in practice these effects will not generally lead to a large increase in wind-produced X-rays. The velocities in overdense wind flows are lower than those in a spherically symmetric wind (Cranmer & Owocki 1996), and so large shock jump velocities and high-temperature shocks are less likely to be produced in overdense wind flows. In the line-force instability model, wind filling factors are smaller in dense winds than in low-density winds, so that dense regions of a stellar wind are unlikely to produce significant excess X-ray emission (Cooper 1994). Furthermore, the existence of fast, low-density streams and slower, denser streams in the same stellar wind does not automatically lead to strong shock interactions between the streams. For example, oblique shocks that occur when the stellar wind interacts with an equatorial disk do not have sufficient velocity differences to produce significant X-ray–emitting plasma (Bjorkman & Cassinelli 1993). One possible excep-

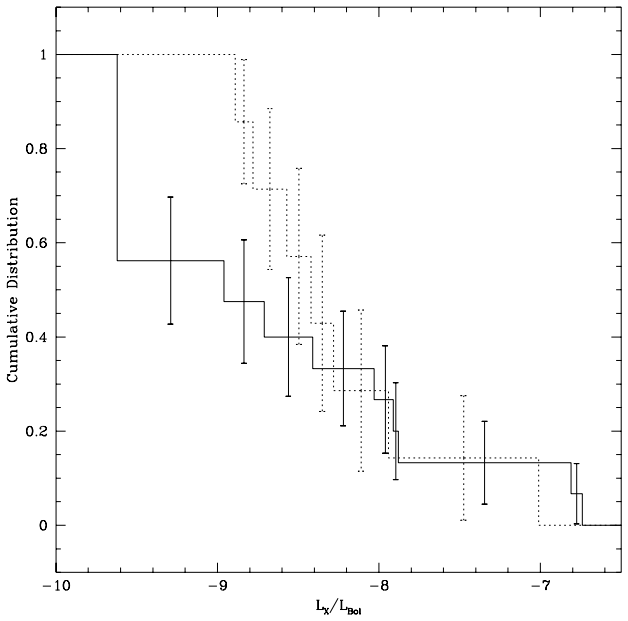

FIG. 4.—Cumulative L_X/L_{Bol} distributions of the Be stars (*dotted line*) and non-Be B V stars with spectral type B1.5 or later (*solid line*).

tion is in the corotating interaction regions that may occur in wind streams over starspots on rotating hot stars (Cranmer & Owocki 1996).

Finally, we may ask whether the two special types of stars in our sample, Be stars and β Cephei variables, have X-ray properties that differ from the normal B V stars. If so, it might imply that rotation, circumstellar material, or pulsation plays an important role in X-ray production in early-type stars. Unfortunately, it is difficult to make a fair comparison between the β Cephei variables and the other stars because β Cephei variables all fall within the same small region of the H-R diagram, and very few stars of similar spectral subtype and luminosity class are not β Cephei variables. However, the X-ray luminosities of the β Cephei variables lie between those of the B0 stars and those of the mid-B stars, as would be expected, and with the exception of ξ^1 CMa, they have soft X-ray spectra similar to the other B V stars in our sample. A further investigation of the temporal properties of the X-ray emission of β Cephei variables has been carried out by Finley, Cohen, & Cassinelli (1997) with much longer observations. These authors present evidence for modulation of the X-rays with periods consistent with the observed optical variability.

The Be stars in our sample fall mostly in the mid-B spectral subtypes, and a comparison between their properties and the properties of the normal B V stars of similar spectral type may shed some light on the X-ray production mechanism of all of the B V stars. Of the 22 stars with spectral type B1.5 or later, 15 are non-Be stars, and only eight of these are detected. In contrast, all seven of the Be stars, including α Col (B7 IV), are detected. We may ask if these two groups, Be stars and normal B V stars with spectral type B1.5 or later, have X-ray luminosities drawn from the same parent distribution. We considered the quantity L_X/L_{Bol} for this comparison in an attempt to negate the spectral type dependence of the X-ray luminosity. We used the ASURV survival analysis software package (Feigelson & Nelson 1985) to apply four different statistical tests to the L_X/L_{Bol} distributions of the Be and the B V stars. These tests showed only marginal statistical significance, with the null hypothesis that there is no difference between the two distributions being rejected with a probability that ranged between 70% and 92%. However, we also used the Kaplan-Meier estimator implemented in ASURV to reconstruct the cumulative luminosity distributions of the two samples. It was necessary to use this technique because of the nondetections in the B V star subsample. We show the reconstructed distributions in Figure 4. Note that the distributions are similar at the bright end, but they diverge at the low end. The median L_X/L_{Bol} value for the Be stars is about 3 times larger than that of the normal B V stars.

It is conceivable that, in general, there is less spread in the X-ray luminosities of Be stars than in the distribution of X-ray luminosities of non-Be B V stars. It could be that the rapid rotation, disks, or pulsation enhance(s) the X-ray production mechanism. An alternative explanation is that UV wind signatures in Be winds persist to later spectral subtypes (Grady, Bjorkman, & Snow 1987), and so filling factors may be the same, but Be stars have larger $\dot{M}/v_\infty$ and thus larger L_X. This implies that the Be stars that are B1.5 or B2 may have wind-shock X-rays to a degree that non-emission B stars of the same spectral subtype would not, even if they have comparable wind filling factors.

7. CONCLUSIONS

Long-duration, pointed *ROSAT* PSPC observations of 27 near–main-sequence B stars that have low interstellar column densities have revealed 20 X-ray sources with luminosities ranging from $L_X = 5.6 \times 10^{27}$ to $L_X = 2.2 \times 10^{32}$. Most of the X-ray spectra are soft, and all are well described by thermal emission models having continuous temperature distributions (DEMs) that are heavily weighted to cooler plasma temperatures. Wind attenuation is included in the spectral models and is found to be important for the three stars with the densest winds. The X-ray fluxes from all of the stars are quite constant, with only two stars showing marginal variability at the 10%–20% level.

We find that a general wind-shock picture can explain the observed X-ray properties of most of the very early (B0 and B1) B V stars in our sample, but only if the theoretical mass-loss rates for these stars are underestimated by a factor of a few. However, X-rays from stars later than about B1.5, as well as the unusual star τ Sco, are very difficult to explain in the context of any reasonable wind-shock scenario. Youth and the properties associated with Be stars may have some bearing on the production of X-rays in sources too strong to be explained in terms of wind shocks.

Some of the questions raised here regarding the origins of X-ray emission in mid-B V stars and the transition from the X-ray properties of very early B V stars to these later spectral subtypes could be addressed with further observations and modeling. The unusual sources such as τ Sco are generally distant and therefore have low fluxes, so a dedicated project to observe a larger sample of mid- and late-B V stars with a next-generation high-throughput X-ray telescope would provide a more robust estimate of some of the properties that we have begun to use as discriminants of the X-ray production mechanism. Furthermore, searches for correlations between X-ray properties and age would be useful in constraining models of X-ray production in B V stars. Finally, a reanalysis of the mass-loss rates of B V stars, taking X-ray photoionization of the stellar winds into

account, might help resolve the filling factor discrepancy in the very early B V stars.

We would like to thank Karen Bjorkman, John Finley, Wilt Sanders, Jon Bjorkman, Glenn Cooper, Barry Welsh, and Stan Owocki for many fruitful discussions. This research has made use of the SIMBAD database, operated at CDS, Strasbourg, France, and was supported by NASA grants NAG5-1579, NAGW-2210, and NAS5-32646 to the University of Wisconsin.

APPENDIX A

TIME VARIABILITY ANALYSIS

In some cases, the several kilosecond long observations were taken nearly continuously, and in other cases, they were split into several sections spanning periods of days and, in a few cases, years. Because the spacecraft wobble—employed to prevent point sources from being obscured by window support wires—can introduce a periodic signal at about 400 s and less, we generally tested only for longer periods. When several discrete observations were separated by more than a few kiloseconds, we compared the count rates of each observation in order to test for longer term variability. For the more nearly continuous observations, we binned the data into 402 s bins in order to average over the wobble period. For longer observations and observations with gaps, we made additional light curves with coarser binning. We stress that because of the wobble period, and also due to the modest time coverage, our data are only capable of showing significant evidence of variability on a narrow range of timescales (a few 10^2–10^4 s and, in a few instances, over timescales of a year, but with very sparse sampling).

We performed time variability analyses only on those eight stars for which we collected sufficient data to form a high signal-to-noise ratio light curve. We did not test for periodic variability associated with β Cephei pulsations, which occurs on timescales of $\sim$6 hr. This issue is explored in Finley et al. (1997).

For all light curves, we first tested the null hypothesis where the data are produced by a constant source. We calculated the χ^2 statistic for each light curve and a model of a constant source with a count rate equal to the weighted mean of all of the data points. The probability that a χ^2 value smaller than that found would be obtained for a truly constant source—roughly interpreted as the probability, $P(\chi^2, \nu)$, that the source is variable—is given in Table C-4 of Bevington (1969). We consider data sets with $P(\chi^2, \nu) > 0.95$ to exhibit significant evidence of source variability. The χ^2 and corresponding $P(\chi^2, \nu)$ values for the 402 s bin light curves are given in Table 8, along with the weighted means and the weighted standard deviations,

$$s = \sqrt{\left[\sum_{i=1}^{N} \frac{(x_i - \mu)^2}{\sigma_i^2}\right] \Big/ \left(\sum_{i=1}^{N} \frac{1}{\sigma_i^2}\right)}, \tag{A1}$$

which are a generic indicator of the degree of variation in the data. We also show the weighted mean uncertainty in the data,

$$\langle \sigma \rangle = \sum_{i=1}^{N} \frac{1}{\sigma_i} \Big/ \sum_{i=1}^{N} \frac{1}{\sigma_i^2}, \tag{A2}$$

as a measure of the variation in the data due to statistical fluctuations.

Only two of the data sets have indications of variability: μ Cen and the β Cen observation taken without the boron filter. None of the other stars show any indication of variability when the light curves are made with larger bins or if the total count rates of each separate observation are compared with each other.

The μ Cen data consist of four observations of approximately 1 ks separated by several 10^4 s. Looking at the four subsets individually, only the third observation shows statistically significant variability. When we considered the mean count rates of the four separate observations, the hypothesis of a constant source generating the data could be rejected at the 94% level. So there appears to be some evidence for variability in the μ Cen data on timescales of a few hundred seconds and up to a few

TABLE 8

VARIABILITY IN X-RAY LIGHT CURVES WITH 402 s BINS

Star	t_{exp} (s)	N	χ^2_ν	$P(\chi^2, \nu)$[a]	μ (counts s^{-1})	s[b] (counts s^{-1})	$\langle\sigma\rangle$[c] (counts s^{-1})	s/μ
τ Sco	2596	9	0.69	0.30	1.704	0.063	0.074	0.04
θ Car	1504	4	1.22	0.70	0.369	0.031	0.032	0.08
β Cen[d]	2863	11	2.55	> 0.99	1.098	0.101	0.064	0.09
β Cen[e]	4449	14	1.07	0.65	0.162	0.023	0.023	0.14
ξ^1 CMa.....	1991	5	1.78	0.88	0.100	0.020	0.017	0.20
α Vir[e]	5422	16	1.35	0.85	0.124	0.023	0.020	0.19
λ Sco.....	1384	5	0.79	0.45	0.462	0.034	0.039	0.07
δ Lup	3210	9	1.32	0.80	0.056	0.018	0.016	0.32
μ Cen	4681	13	2.16	> 0.99	0.044	0.018	0.012	0.41

[a] The probability with which the null hypothesis can be rejected.
[b] The weighted standard deviation of the data.
[c] The weighted mean of the statistical uncertainty of the data.
[d] Data taken without the boron filter.
[e] Data taken with the boron filter.

10^4 s. We also tested for variability in light curves made from only hard counts (energy channels 50–201) and from only soft counts (channels 11–40). The "hard" light curve showed marginal variability (null hypothesis rejected at the 93% level), whereas the "soft" light curve did not display any variability.

Whether the X-rays are generated in wind shocks or in coronal plasma, the process is complex and is likely to lead to variability with both stochastic and periodic components. Absent a specific model, we choose to quantify the amplitude of the variability by examining the ratio of the variance to the mean, s/μ. This value will be inflated because of statistical errors. For that reason, we calculated the mean statistical uncertainty, $\langle\sigma\rangle$, in order to provide an estimate of the fraction of the variation that is due to measurement uncertainties. The variance of the 402 s bin light-curve data for μ Cen is 40% of the mean and is significantly larger than the mean measurement error per datum, implying that this figure is not dominated by statistical uncertainty. For the distribution of the mean count rates of the four separate observations, the amplitude as given by the variance is 20%. Again, the measurement error is small compared with this. This implies that the variability is primarily, but not entirely, on timescales less than a few 10^4 s.

The β Cen data consists of several groups of short observations (a few hundred seconds) with a half-year gap between the two observing seasons. While the boron filter observations do not show any variability, the unfiltered ones do. This is likely due to the better signal-to-noise ratio of the unfiltered data. The mean count rates of the two sections of data taken a half-year apart are consistent with each other; however, there is evidence of variability on all the shorter timescales that we sampled. The 402 s light curve is inconsistent with a constant source at better than the 99% level. The light curve consisting of the means of the six discontinuous sections also indicates variability at the 97% confidence level. Significant variability for β Cen occurs only in the data from the second observing season.

The variance of the β Cen data in the 402 s bin light curve is about 10% of the mean, and the peak-to-peak variation (again, only including bins with detector on-time exceeding 200 s) is about 15% of the mean count rate. For the light curve with the larger 5000 s bins, the variance is also about 10% of the mean. We therefore cannot state whether the variability is stronger on $\sim 10^3$ s timescales or on $\sim 10^4$ s timescales. When we subdivided the counts into soft and hard light curves, we found that only the soft light curve showed significant variability, and even then only on short ($\sim 10^3$ s) timescales. Of course, the lower signal-to-noise ratios in these soft and hard light curves make it more difficult to detect variability.

In summary, only two of the eight stars show any indication of variability, with the upper limits of the variability amplitudes of the other six stars being in some cases less than 10%. The variability in β Cen is minor, with an amplitude of about 10% as given by the ratio of the variance to the mean count rate. The variability in μ Cen is not significantly stronger, but the timescale appears to be shorter.

REFERENCES

Abbott, D. C. 1982, ApJ, 259, 282
Anders, E., & Grevesse, N. 1989, Geochim. Cosmochim. Acta, 53, 197
Ayres, T. R., Linsky, J. L., Vaiana, G. S., Golub, L., & Rosner, R. 1981, ApJ, 250, 293
Berghöfer, T. W., & Schmitt, J. H. M. M. 1994a, A&A, 292, 5
———. 1994b, Science, 265, 1689
Berghöfer, T. W., Schmitt, J. H. M. M., Danner, R., & Cassinelli, J. P. 1997, A&A, 322, 167
Bevington, P. R. 1969, Data Reduction and Error Analysis in the Physical Sciences (New York: MacGraw-Hill)
Bjorkman, J. E., & Cassinelli, J. P. 1993, ApJ, 409, 429
Bjorkman, J. E., Ignace, R., Tripp, T. M., & Cassinelli, J. P. 1994, ApJ, 435, 416
Bohlender, D. A. 1994, in Pulsation, Rotation, and Mass Loss in Early-Type Stars, ed. L. A. Balona, H. F. Henrichs, & J. M. Le Contel (Dordrecht: Kluwer), 155
Briceño, C., Hartmann, L. W., Stauffer, J. R., Gagne, M., Stern, R. A., & Caillault, J.-P. 1997, AJ, 113, 740
Briot, D., & Zorec, J. 1994, in Pulsation, Rotation, and Mass Loss in Early-Type Stars, ed. L. A. Balona, H. F. Henrichs, & J. M. Le Contel (Dordrecht: Kluwer), 356
Cassinelli, J. P., Cohen, D. H., MacFarlane, J. J., Sanders, W. T., & Welsh, B. Y. 1994, ApJ, 421, 705 (Paper I)
Cassinelli, J. P., & Swank, J. H. 1983, ApJ, 271, 681
Cassinelli, J. P., Waldron, W. L., Sanders, W. T., Harnden, F. R., Rosner, R., & Vaiana, G. S. 1981, ApJ, 250, 677
Castor, J. I., Abbott, D. C., & Klein, R. I. 1975, ApJ, 195, 157
Chlebowski, T., Harnden, F. R., Jr., & Sciortino, S. 1989, ApJ, 341, 427
Cohen, D. H., Cassinelli, J. P., & Waldron, W. L. 1997, ApJ, 488, in press
Cohen, D. H., Cooper, R. G., MacFarlane, J. J., Owocki, S. P., Cassinelli, J. P., & Wang, P. 1996, ApJ, 460, 506
Cooper, R. G. 1994, Ph.D. thesis, Univ. Delaware
Corcoran, M. F., et al. 1993, ApJ, 412, 792
Cranmer, S. R., & Owocki, S. P. 1996, ApJ, 462, 469
Dachs, J., & Hummel, W. 1996, A&A, 312, 818
Drew, J. E. 1989, ApJS, 71, 267
Feigelson, E. D., & Nelson, P. I. 1985, ApJ, 293, 192
Feldmeier, A. 1995, A&A, 299, 523
Feldmeier, A., Kudritzki, R. P., Palsa, R., Pauldrach, A. W. A., & Puls, J. 1997a, A&A, 320, 899
Feldmeier, A., Puls, J., & Pauldrach, A. W. A. 1997b, A&A, in press
Finley, J. P., Cohen, D. H., & Cassinelli, J. P. 1997, in preparation
Freire Ferrero, R., Gouttebroze, P., Catalano, S., Marilli, E., Bruhweiler, F., Kondo, Y., van der Hucht, K., & Talaver, A. 1995, ApJ, 439, 1011
Fruscione, A., Hawkins, I., Jelinsky, P., & Wiercigroch, A. 1994, ApJS, 94, 127
Geis, D. R., & Lambert, D. L. 1992, ApJ, 387, 673
Grady, C. A., Bjorkman, K. S., & Snow, T. P. 1987, ApJ, 320, 376
Grillo, F., Sciortino, S., Micela, G., Vaiana, G. S., & Harnden, F. R., Jr. 1992, ApJS, 81, 795
Haisch, B., & Schmitt, J. H. M. M. 1996, PASP, 108, 113
Haisch, B., & Simon, T. 1982, ApJ, 263, 252
Hanbury Brown, R., Davis, J., & Allen, L. R. 1974, MNRAS, 167, 121
Hillier, D. J., Kudritzki, R. P., Pauldrach, A. W. A., Baade, D., Cassinelli, J. P., Puls, J., & Schmitt, J. H. M. M. 1993, A&A, 276, 117
Hiltner, W. A., Garrison, R. F., & Schild, R. E. 1969, ApJ, 157, 313
Hoffleit, D., & Jaschek, C. 1982, The Bright Star Catalog (New Haven: Yale Univ. Press)
Ignace, R., Cassinelli, J. P., & Bjorkman, J. E. 1996, ApJ, 459, 671
Kaper, L., Henrichs, H. F., Nichols, J. S., Snoek, L. C., Volten, H., & Zwarthoed, G. A. A. 1996, A&AS, 116, 257
Kilian, J. 1992, A&A, 262, 171
Kiriakidis, M., El Eid, M. F., & Glatzel, W. 1992, MNRAS, 225, 1P
Kudritzki, R. P., Hummer, D. G., Pauldrach, A. W. A., Puls, J., Najarro, F., & Imhoff, J. 1992, A&A, 257, 655
Kudritzki, R. P., Palsa, R., Feldmeier, A., Puls, J., & Pauldrach, A. W. A. 1996, in MPE Rep. 263, Röntgenstrahlung from the Universe, ed. H. U. Zimmermann, J. Trümper, & H. York (Garching: MPE), 9
Kudritkzi, R. P., Pauldrach, A., Puls, J., & Abbott, D. C. 1989, A&A, 219, 205
Lamers, H. J. G. L. M., & Rogerson, J. B. 1978, A&A, 66, 417
Lampton, M., Margon, B., & Bowyer, S. 1976, ApJ, 208, 177
Lesh, J. R. 1968, ApJS, 17, 371
Lucy, L. B. 1983, ApJ, 274, 372
Lucy, L. B., & Solomon, P. M. 1970, ApJ, 159, 879
MacFarlane, J. J., & Cassinelli, J. P. 1989, ApJ, 347, 1090
MacFarlane, J. J., Cohen, D. H., & Wang, P. 1994, ApJ, 437, 351
MacFarlane, J. J., Waldron, W. L., Corcoran, M. F., Wolff, M. J., & Wang, P. 1993, ApJ, 419, 813
Massa, D., et al. 1995, ApJ, 452, L53
Meurs, E. J. A., et al. 1992, A&A, 265, L41
Mewe, R., Kaastra, J. S., & Liedahl, D. A. 1995, Legacy, 6, 16
Morrison, R., & McCammon, D. 1983, ApJ, 270, 119
Moskalik, P., & Dziembowski, W. 1992, A&A, 256, L5
Mullan, D. J. 1984, ApJ, 283, 303
Nousek, J. A., & Lesser, A. 1993, *ROSAT* Newsl., Vol. 8
Owocki, S. P., Castor, J. I., & Rybicki, G. B. 1988, ApJ, 335, 914
Pallavicini, R., Golub, L., Rosner, R., Vaiana, G. S., Ayers, T., & Linsky, J. L. 1981, ApJ, 248, 279
Pfeffermann, E., et al. 1986, Proc. SPIE, 733, 519
Prinja, R. K., Massa, D., Fullerton, A. W., Howarth, I. D., & Pontefract, M. 1997, A&A, 318, 157

Raymond, J. C., & Smith, B. W. 1977, ApJS, 35, 419
Runacres, M. C., & Blomme, R. 1996, A&A, 309, 554
Schmitt, J. H. M. M., Collura, A., Sciortino, S., Vaiana, G. S., Harnden, F. R., & Rosner, R. 1990, ApJ, 365, 704
Schmitt, J. H. M. M., & Snowden, S. L. 1990, ApJ, 361, 207
Schmitt, J. H. M. M., Zinnecker, H., Cruddace, R., & Harnden, F. R. 1993, ApJ, 402, L13
Smith, M. A. 1980, in Nonradial and Nonlinear Stellar Pulsations, ed. H. A. Hill & W. Dziembowski (Berlin: Springer), 60
Smith, M. A., Grady, C. A., Peters, G. J., & Feigelson, E. D. 1993, ApJ, 409, L49
Smith, M. A., Hubeny, I., Lanz, T., & Meylan, T. 1994, ApJ, 432, 392
Sterken, C., & Jerzykiewicz, M. 1993, Space Sci. Rev., 62, 95
Straizys, V., & Kuriliene, G. 1981, Ap&SS, 80, 353
Telting, J. H., Heemskerk, M. H. M., Henrichs, H. F., & Savonije, G. J. 1994, A&A, 288, 558
Tout, C. A., & Pringle, J. E. 1995, MNRAS, 272, 528
Trümper, J. 1983, Adv. Space Res., 2(4), 241
Uesugi, A., & Fukuda, I. 1982, Revised Catalog of Stellar Rotational Velocities (Kyoto: Kyoto Univ.)
Vacca, W. D., Garmany, C. D., & Shull, J. M. 1996, ApJ, 460, 914
Waelkens, C., & Rufener, F. 1985, A&A, 152, 6
Walborn, N. R., Parker, J. W., & Nichols, J. S. 1995, NASA Ref. Publ. 1363
Walter, F. M., Matthews, L. D., & Linsky, J. L. 1995, ApJ, 447, 353
Wang, P., Cohen, D. H., & MacFarlane, J. J. 1997, in preparation
Waters, L. B. F. M., & Marlborough, J. M. 1994, in Pulsation, Rotation, and Mass Loss in Early-Type Stars, ed. L. A. Balona, H. F. Henrichs, & J. M. Le Contel (Dordrecht: Kluwer), 399
Waters, L. B. F. M., Marlborough, J. M., Geballe, T. R., Oosterbroek, T., & Zaal, P. 1993, A&A, 272, 9
Welsh, B. Y. 1991, ApJ, 373, 556
Welsh, B. Y., Craig, N., Vedder, P. W., & Vallerga, J. V. 1994, ApJ, 437, 638
Wood, K., Bjorkman, K. S., & Bjorkman, J. E. 1997, ApJ, 477, 926